

## INFORMATION TO USERS

The most advanced technology has been used to photograph and reproduce this manuscript from the microfilm master. UMI films the text directly from the original or copy submitted. Thus, some thesis and dissertation copies are in typewriter face, while others may be from any type of computer printer.

The quality of this reproduction is dependent upon the quality of the copy submitted. Broken or indistinct print, colored or poor quality illustrations and photographs, print bleedthrough, substandard margins, and improper alignment can adversely affect reproduction.

In the unlikely event that the author did not send UMI a complete manuscript and there are missing pages, these will be noted. Also, if unauthorized copyright material had to be removed, a note will indicate the deletion.

Oversize materials (e.g., maps, drawings, charts) are reproduced by sectioning the original, beginning at the upper left-hand corner and continuing from left to right in equal sections with small overlaps. Each original is also photographed in one exposure and is included in reduced form at the back of the book. These are also available as one exposure on a standard 35mm slide or as a 17" x 23" black and white photographic print for an additional charge.

Photographs included in the original manuscript have been reproduced xerographically in this copy. Higher quality 6" x 9" black and white photographic prints are available for any photographs or illustrations appearing in this copy for an additional charge. Contact UMI directly to order.

# U·M·I

University Microfilms International  
A Bell & Howell Information Company  
300 North Zeeb Road, Ann Arbor, MI 48106-1346 USA  
313/761-4700 800/521-0600



**Order Number 9013138**

**S-parameter VLSI transmission line analysis**

**Cooke, Bradly James, Ph.D.**

**The University of Arizona, 1989**

**Copyright ©1989 by Cooke, Bradly James. All rights reserved.**

**U·M·I**  
300 N. Zeeb Rd.  
Ann Arbor, MI 48106



S-PARAMETER VLSI TRANSMISSION LINE ANALYSIS

by

Bradly James Cooke

---

Copyright ©Bradly James Cooke 1989

A Dissertation Submitted to the Faculty of the  
DEPARTMENT OF ELECTRICAL AND COMPUTER ENGINEERING

In Partial Fulfillment of the Requirements  
for the Degree of

DOCTOR OF PHILOSOPHY  
WITH A MAJOR IN ELECTRICAL ENGINEERING

in the Graduate College


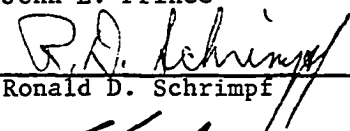
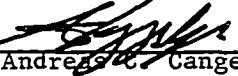
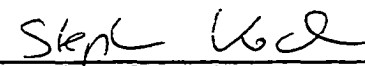

THE UNIVERSITY OF ARIZONA

1 9 8 9

THE UNIVERSITY OF ARIZONA  
GRADUATE COLLEGE

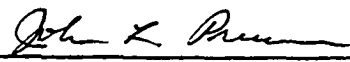
As members of the Final Examination Committee, we certify that we have read  
the dissertation prepared by Bradly James Cooke  
entitled S-PARAMETER VLSI TRANSMISSION LINE ANALYSIS

and recommend that it be accepted as fulfilling the dissertation requirement  
for the Degree of Doctor of Philosophy.

<u></u> John L. Prince	<u>10/27/89</u> Date
<u></u> Ronald D. Schrimpf	<u>10/27/89</u> Date
<u></u> Andrej Cangelaris	<u>10/27/89</u> Date
<u></u> Stephan W. Koch	<u>10/27/89</u> Date
<u></u> John D. McCullen	<u>10/27/89</u> Date

Final approval and acceptance of this dissertation is contingent upon the  
candidate's submission of the final copy of the dissertation to the Graduate  
College.

I hereby certify that I have read this dissertation prepared under my  
direction and recommend that it be accepted as fulfilling the dissertation  
requirement.

<u></u> Dissertation Director John L. Prince	<u>11/27/89</u> Date
--	-------------------------

## STATEMENT BY AUTHOR

This dissertation has been submitted in partial fulfillment of requirements for an advanced degree at The University of Arizona and is deposited in the University Library to be made available to borrowers under rules of the Library.

Brief quotations from this dissertation are allowable without special permission, provided that accurate acknowledgment of source is made. Requests for permission for extended quotation from or reproduction of this manuscript in whole or in part may be granted by the copyright holder.

SIGNED: \_\_\_\_\_

*Booke*

### ACKNOWLEDGMENT

Trust In The Lord For He Shall Provide.

First and foremost I would like to thank the two ladies in my life whose support has been most crucial; my mother, Irma Cooke and my wife Dr. Ann S. Copenhaver (Cooke). My mother has from the very beginning of my life given me the guidance and instilled the values that has shaped the person I have become. In raising four kids in Central and South America and latter in Arizona, she has set an example in courage and perseverance that I have and will always be able to fall back on. Ann, in recent years, has been a very important part of my life. She has provided both physical and emotional support during my graduate career. Her seemingly endless confidence in my abilities, continuing encouragement and love have played an important part in this dissertation.

Next, over my graduate student years I have been influenced by many professors both academically and personally. However, several professors have left their imprint upon me more than any others in a very special way. In the order of their chronological influence I would like to acknowledge:

Dr. B. Wilamowski for encouraging me to think in a unique manner and starting me on my way through graduate school.

Dr. D. J. Hamilton for setting an example of what it is to be a scholar and a gentleman. While I may never be able to duplicate his accomplishment, I know through his example the direction and the standard I will always strive for.

Dr. J. L. Prince. Through him I have learned some of the intricacies of academic politics, developed the strength of character to stand fast on by beliefs and sharpened by abilities to think critically and objectively. These are priceless skills which will now and in the future become as important as understanding the basic academics of my chosen field.

## TABLE OF CONTENTS

LIST OF ILLUSTRATIONS . . . . .	7
ABSTRACT . . . . .	9
1. INTRODUCTION . . . . .	10
2. S-PARAMETER CIRCUIT ANALYSIS . . . . .	14
2.1 Frequency Domain S-parameters . . . . .	14
2.2 Frequency Domain Circuit Analysis . . . . .	16
2.3 Time Domain Circuit Analysis . . . . .	22
3. FREQUENCY DEPENDENT S-PARAMETER MODELS . . . . .	23
3.1 Frequency Dependent R,L,C Element S-parameters . . . . .	23
3.2 Frequency Dependent Quasi-TEM Transmission Lines . . . . .	25
3.3 Frequency Dependent Non-TEM Transmission Lines . . . . .	34
4. NON-LINEAR TERMINATIONS . . . . .	36
4.1 Transforming S-parameters to Y-parameters . . . . .	36
4.2 Y-parameter Time Domain Analysis . . . . .	41
5. INCORPORATION OF EXTERNALLY GENERATED S-PARAMETERS . . . . .	44
5.1 Processing externally generated S-parameters . . . . .	44
6. SPECTRAL COMPOSITION OF A PULSE . . . . .	47
6.1 Trigonometric Fourier Series of a General Pulse . . . . .	47
6.2 Integral-Squared Error of a Pulse . . . . .	51
6.3 Estimation of Pulse Spectrum and Required System Bandwidth . . . . .	53
7. S-PARAMETER ANALYSIS OF INTERCONNECT DISCONTINUITIES . . . . .	58
7.1 Poynting's Theorem . . . . .	58
7.2 Application of Poynting's Theorem to a Discontinuity. . . . .	61
7.3 S-parameter Network Models of Interconnect Discontinuities . . . . .	64
8. IMPLEMENTATION OF THE S-PARAMETER ANALYSIS TECHNIQUE . . . . .	71
8.1 System Overview . . . . .	71
8.2 Architecture . . . . .	73
8.3 Numerical Techniques . . . . .	74
8.4 Fourier Aliasing (Error Analysis) . . . . .	75
9. EXPERIMENTAL MEASUREMENT AND SIMULATION COMPARISON . . . . .	80
9.1 Experimental S-parameter Measurements . . . . .	80
9.2 Simulation . . . . .	82
10. CONCLUSION . . . . .	97

TABLE OF CONTENTS - Continued

6

APPENDIX A: S-PARAMETER APPLICATIONS . . . . .	98
REFERENCES . . . . .	105

### LIST OF ILLUSTRATIONS

Figure 1. S-parameter formulation of a linear multiport network. . . . .	15
Figure 2. S-parameter network composed of m components. . . . .	17
Figure 3. Two port S-parameter representation of an impedance and two port S-parameter representation of a transmission line of length l. . . . .	24
Figure 4. 2N port S-parameter representation of a N coupled transmission line. . . . .	29
Figure 5. Network used for S-parameter impedance transformation and S-parameter to Y-parameter conversion. . . . .	37
Figure 6. Augmented network used to cancel old termination $Z_0$ and introduce nonlinear terminations Z. . . . .	42
Figure 7. Waveform used for the derivation of the general Fourier series of a pulse. . . . .	48
Figure 8. Number of fourier terms as a function of percent rise time and fall time for a 50% duty cycle and 1%, 0.5% and 0.1% integral-squared error. . . . .	54
Figure 9. Plot of 10% rise and fall time pulse with four and seven term approximation corresponding to 1% and 0.1% integral-squared error. . . . .	56
Figure 10. A transmission line network and system transfer function. . . . .	57
Figure 11. A discontinuity region defined by a the volume V and bounded by the surface S between two transmission line segments $T_1$ and $T_2$ . . . . .	62
Figure 12. Series impedance S-parameters. . . . .	65
Figure 13. Shunt admittance S-parameters. . . . .	66
Figure 14. T-network S-parameters. . . . .	67
Figure 15. Pi-network S-parameters. . . . .	68
Figure 16. Equivalent T-network circuit or a bend and via. . . . .	69

**LIST OF ILLUSTRATIONS - Continued**

8

Figure 17. Architecture of the implemented algorithm. . . . .	72
Figure 18. The top figure shows a correctly sampled signal, while the bottom figure shows the aliasing effects of under sampling the signal. . . . .	78
Figure 19. Thin film multilayer high frequency test structure. . .	81
Figure 20. S11, S12 S-parameter measurement, h=10 $\mu\text{m}$ . . . . .	83
Figure 21. S11, S12 S-parameter measurement, h=20 $\mu\text{m}$ . . . . .	84
Figure 22. S11, S12 S-parameter simulation, h=10 $\mu\text{m}$ . . . . .	91
Figure 23. S11, S12 S-parameter simulation, h=20 $\mu\text{m}$ . . . . .	92
Figure 24. Time domain propagation of pulse for 50 $\Omega$ terminations. . . . .	93
Figure 25. Network schematic of time domain simulation. . . . .	95
Figure 26. Network response for 100 MHz clock with 0.1 ns rise time. . . . .	96
Figure 27. Transmission line system used to illustrate effects of line losses. . . . .	99
Figure 28. 10 MHz pulse train far end response (node A). . . . .	100
Figure 29. 100 MHz pulse train far end response (node A). . . . .	101
Figure 30. The equivalent two port macro for a microstrip bend. . .	103
Figure 31. Coupled five conductor microstrip simulation with using macros. . . . .	104

**ABSTRACT**

This dissertation investigates the implementation of S-parameter based network techniques for the analysis of multiconductor, high speed VLSI integrated circuit and packaging interconnects. The S-parameters can be derived from three categories of input parameters: 1) lossy quasi-static R,L,C and G, 2) lossy frequency dependent (dispersive) R,L,C,G and 3) the propagation constants,  $\Gamma$ , the characteristic impedance,  $Z_c$  and the conductor eigencurrents,  $I$ , derived from full wave analysis. The S-parameter network techniques developed allow for: the analysis of periodic waveform excitation, the incorporation of externally measured or calculated scattering parameter data and large system analysis through macro decomposition. The inclusion of non-linear terminations has also been developed.

## CHAPTER 1

### INTRODUCTION

Analysis of electrical interconnect structures has become an important requirement in the design of high speed digital and analog systems. Electrical interconnects can, in a simplistic fashion, be defined as the electrically conductive elements used to connect a signal source to a signal receiver. Technological advances in the microelectronic industry have allowed for increasing miniaturization of integrated circuit (IC) geometries leading to higher interconnect densities, larger Input/Output (IO) count and faster signal speeds. Faster signal speeds have led to the requirement that interconnects be treated as transmission lines while the increased interconnect densities compound analysis problems due to the effects of coupling between interconnect elements. In addition, integrated circuit processing and layout rules tend to limit the range of materials and structural techniques available in the design of interconnects, leading to signal deterioration due to dispersion and discontinuities. In summary, as VLSI interconnect density, complexity and signal speed increase, interconnect transmission line effects such as dispersion, propagation delay, termination mismatch, discontinuities and coupling become more pronounced. If neglected, such effects may lead, through signal deterioration, to an electronic system failure or to suboptimal cost, performance or manufacturability. Therefore, an effort

to fully understand the interconnect problem through theoretical analysis and modeling becomes important.

The analysis of transmission lines can be divided into the following three general categories<sup>1</sup>. The first, the quasi-static model, assumes the propagating mode to be purely TEM in nature, that is, the electric and magnetic fields lie in the transverse plane perpendicular to the direction of propagation. The transmission line is characterized by its equivalent electrostatic capacitance, inductance, conductance and in an ad hoc manner, its ohmic resistance. The next category, the dispersion model, allows for deviations from the quasi-static model by allowing its parameters (R,L,C,G) to vary with frequency. The final category makes use of fullwave analysis techniques to determine the frequency dependent modal propagation constant, characteristic impedance and any other required parameters. Traditionally, transmission line analysis of VLSI electronic systems has been primarily limited to category 1 analysis due to the time domain nature of their simulation. Typically the system transient response is found by solving the Telegraphist wave equation with quasi-static parameters in the time domain. Category 2 or the dispersive models can be developed if the Telegraphist wave equation is solved in the frequency domain with frequency dependent parameters. It should be noted that the Telegraphist wave equation cannot be extended to include category 3 analysis.

The work presented here investigates the implementation of scattering parameter (S-parameter) techniques for the category 1 through

category 3 analysis of high speed integrated circuit and packaging interconnects. S-parameter network analysis has been an important design tool for the microwave engineer since 1960. However, microwave circuits generally have very different system requirements than do high speed digital IC's. Microwave networks tend to operate over a very narrow bandwidth centered about a specific frequency, allowing the engineer to analyze the system at the single center frequency. If necessary, physical modifications to the system can be made to minimize the degenerative effects of coupling or discontinuities at the given operating frequency, enhancing system performance and ease of analysis. Digital IC networks, on the other hand, require analysis over a very wide bandwidth (the signals tend to be in the form of periodic pulses). In addition, due to the lossy nature of materials and high density layout rules used in IC and IC package fabrication, special care must be taken to include frequency dependent line losses, frequency dependent discontinuities and line coupling into account. Hence, the goal of this research was to extend and develop known microwave S-parameter network techniques to handle the time domain and frequency domain response of high speed, frequency dependent integrated circuit and packaging interconnects. Specifically, this required original work in the development of the following: 1) inclusion of multi-port connections to the general S-parameter network analysis framework, 2) S-parameter extraction of frequency dependent lines for analysis categories 1-3 and 3) extension of S-parameter analysis techniques to include non-linear terminations. In addition, the

time/frequency domain relation for VLSI digital signals was analyzed, guidelines for incorporation of externally generated S-parameters were developed and S-parameter network models of interconnect discontinuities were identified and justified.

The dissertation proceeds as follows. First, S-parameters are defined and time and frequency domain network analysis is explained. Next, the S-parameter representation for typical passive elements used in VLSI interconnection systems such as frequency dependent resistors, capacitors and inductors are described. In addition, the  $2N$ -port S-parameter matrix used to represent frequency dependent  $N$ -coupled lines is derived. This is followed by a derivation of a sequence of S-parameter transformations required to implement non-linear terminations and incorporation of externally generated S-parameters. A chapter on the spectral analysis of a digital pulse is included so that the correlation between the time domain parameters of duty cycle, rise time, fall time and clock frequency of the pulse and its related frequency domain power spectrum is understood. This leads to the relationship between the pulse spectrum and the required system bandwidth. Finally, an overview of a computer based implementation of the developed S-parameter techniques is given, followed by experimental comparison and examples.

## CHAPTER 2

## S-PARAMETER CIRCUIT ANALYSIS

S-parameters are wave variables that are useful for the analysis of high frequency networks. This chapter defines the S-parameter and explains how S-parameters are used in frequency and time domain network analysis.

## 2.1 Frequency Domain S-parameters

The scattering parameter (S-parameter or Scattering matrix) formulation is a useful technique for analyzing multiport microwave networks<sup>2,3</sup>. S-parameters represent the relationship between variables  $a_j$  (proportional to the incoming wave at the  $j^{\text{th}}$  port) and the variables  $b_i$  (proportional to the outgoing wave at the  $i^{\text{th}}$  port).

$$b_1 = S_{11}a_1 + S_{12}a_2 + \dots$$

$$b_2 = S_{21}a_1 + S_{22}a_2 + \dots$$

$$\vdots \quad \vdots \quad \vdots$$

In general for an n-port network

$$\mathbf{b} = \mathbf{S}\mathbf{a} \tag{2.1}$$

where  $\mathbf{S}$  is an  $n \times n$  matrix and represents the scatter matrix of the network.

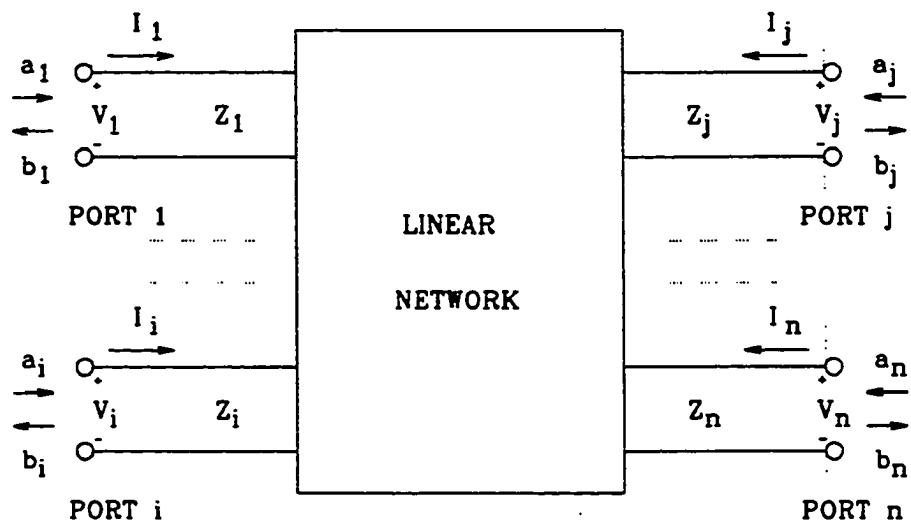


Figure 1. S-parameter formulation of a linear multiport network.

It should be noted that the wave variables  $a_j$  and  $b_i$  are measured at an arbitrary point (see Figure 1) along transmission lines of characteristic impedances  $Z_i$  and  $Z_j$  connected to the  $i^{\text{th}}$  and  $j^{\text{th}}$  port respectively of the multiport network. The effective circuit voltage and current at the  $i^{\text{th}}$  port can be expressed in terms of the forward and reverse traveling waves<sup>4</sup> (for the quasi-TEM case)

$$V_i = V_i^+ + V_i^- = Z_i^{\frac{1}{2}}(a_i + b_i) \quad (2.2)$$

$$I_i = I_i^+ + I_i^- = (a_i - b_i)/Z_i^{\frac{1}{2}}. \quad (2.3)$$

Throughout the rest of this dissertation, the characteristic impedance  $Z_i$  will be set to 1 ohm unless stated otherwise.

## 2.2 Frequency Domain Circuit Analysis

The behavior of circuits may be analyzed in terms of the normalized wave variables at the ports of the component multiports<sup>5</sup>. For a circuit component with  $n_k$  ports as shown in Figure 2, a system of  $n_k$  equations can be written

$$S_k a_k = b_k \quad (2.4)$$

where  $S_k$  is its scattering matrix and  $a_k$  and  $b_k$  represent the vectors of incoming and outgoing waves at its  $n_k$  ports. A source can be included into

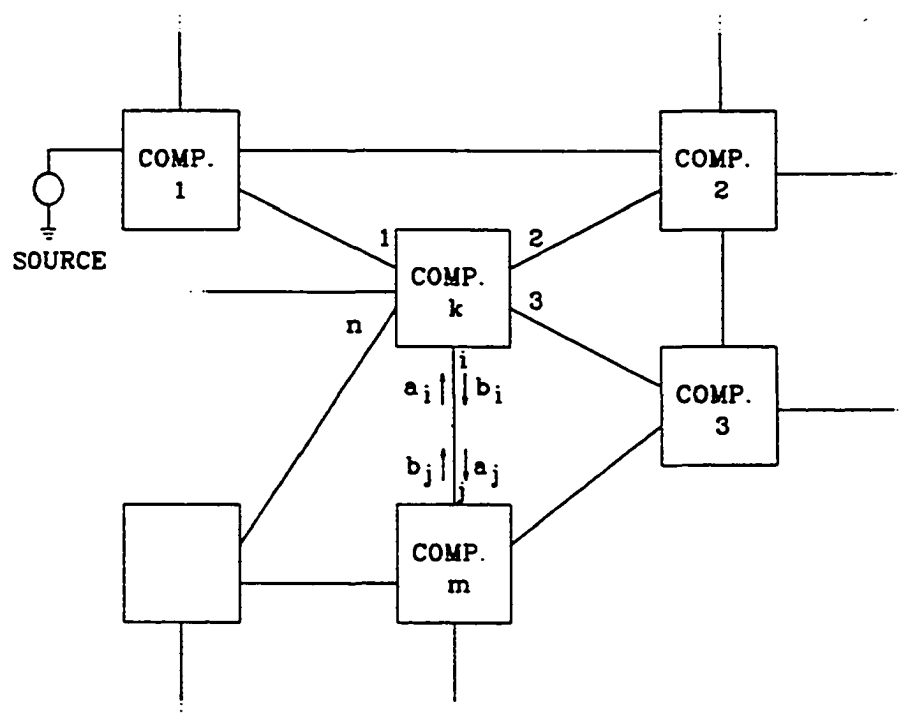


Figure 2. S-parameter network composed of  $m$  components.

the system and is described by the relation

$$b_s = S_s a_s + c_s \quad (2.5)$$

where  $c_s$  is the magnitude and phase of the impressed wave and  $S_s$  is the scatter coefficient of the source ( $S_c=0$  for a matched source).

The overall system equation for all  $n$  components including sources is

$$b = Sa + c \quad (2.6)$$

where  $S$  will be block diagonal and whose  $n$  sub-matrices along the diagonal will correspond to the  $n$  circuit components, and  $a$ ,  $b$  and  $c$  will be row vectors representing incoming, outgoing and impressed waves.

The interconnections of the various components impose constraints on incoming and outgoing waves at the component's port which may be put in the form

$$b = \Gamma a \quad (2.7)$$

where  $\Gamma$  is an  $n \times n$  matrix and represents the interconnection status of the  $a$  and  $b$  waves. The elements of  $\Gamma$  for two or more interconnected ports can

be found by analyzing the properties of a fictitious ideal interconnect element. The desired properties of this ideal interconnect element can be summarized as follows:

- 1) The interconnect contain no preferred current paths
- 2) All interconnect ports must be perfectly matched (no reflections)
- 3) The sum of the interconnect port currents must be consistent with Kirchoff's current law.

Imposing Kirchoff's current law at the ports of an interconnect element composed of  $m$  ports (note  $Z_i=1$  ohm)

$$I_1+I_2+I_3+\dots+I_m=0 \quad (2.8)$$

or, from equation 2.3

$$(a_1-b_1)+(a_2-b_2)+(a_3-b_3)+\dots+(a_m-b_m)=0. \quad (2.9)$$

From  $b=\Gamma a$

$$b_1=a_1\Gamma_{11}+a_2\Gamma_{12}+\dots+a_m\Gamma_{1m}$$

$$b_2=a_1\Gamma_{21}+a_2\Gamma_{22}+\dots+a_m\Gamma_{2m}$$

.....

$$b_m=a_1\Gamma_{m1}+a_2\Gamma_{m2}+\dots+a_m\Gamma_{mm}$$

Substitution into KCL (equation 2.8 and 2.9) gives

$$a_1(1-\Gamma_{11}-\Gamma_{21}-\dots-\Gamma_{m1})+a_2(1-\Gamma_{12}-\Gamma_{22}-\dots-\Gamma_{m2})+\dots+a_m(1-\Gamma_{1m}-\Gamma_{2m}-\dots-\Gamma_{mm})=0$$

To satisfy KCL for all values of  $a_i$  requires that

$$1-\Gamma_{11}-\Gamma_{21}-\dots-\Gamma_{m1}=0$$

$$1-\Gamma_{12}-\Gamma_{22}-\dots-\Gamma_{m2}=0$$

.....

$$1-\Gamma_{1m}-\Gamma_{2m}-\dots-\Gamma_{mm}=0$$

The additional constraint given by the second interconnect element property above (no reflections) requires that  $\Gamma_{ii}=0$  for  $i=1,2,\dots,m$ . With the above two constraints and from the first property (no preferred current path), the elements of the interconnect matrix are

$$\Gamma_{ij}=1/(m-1) \quad \text{for } i,j=1,2,\dots,m \quad i \neq j \quad (2.10)$$

$$\Gamma_{ij}=0 \quad \text{for } i,j=1,2,\dots,m \quad i=j. \quad (2.11)$$

Hence, the elements of  $\Gamma$  are zero if there are no port connections, unity for a single port and  $1/(m-1)$  for  $m$  ports.

Substitution of  $b=\Gamma a$  into  $b=Sa+c$  provides an equation in  $a$

$$(\Gamma-S)a=c \quad (2.12)$$

from which  $a$  can be found in terms of the  $S$ -parameters and the interconnection matrix.  $b$  can then be calculated from equation 2.7.

Application of frequency domain  $S$ -parameter techniques to circuit analysis proceeds as follows. First the time domain input signal  $c(t)$  is subjected to an  $N$  point FFT producing  $c(\omega_i)$ ,  $i=1,2..N$ . Then, after calculating the  $S(\omega_i)$ , the impulse responses of  $a(\omega_i)$  and  $b(\omega_i)$  are found from

$$a(\omega_i)=[\Gamma-S(\omega_i)]^{-1}U \quad (2.13)$$

$$b(\omega_i)=\Gamma a(\omega_i) \quad (2.14)$$

where  $U$  is a unity vector with elements set to 1 (corresponding to unit excitation) or zero.

Finally, the time domain response is found by Inverse Fast Fourier Transforming (IFFT) the sum or difference of  $a(\omega_i)$  and  $b(\omega_i)$  multiplied by  $c(\omega_i)$ , representing voltage and currents respectively

$$V(t)=\text{IFFT}[(a(\omega_i)+b(\omega_i))c(\omega_i)] \quad (2.15)$$

$$I(t)=\text{IFFT}[(a(\omega_i)-b(\omega_i))c(\omega_i)]. \quad (2.16)$$

Note that in utilizing the unit excitation  $U$ , the S-parameters of the overall system can easily be found. By setting  $U_i=1$ , and  $U_j=0$   $i, j=1, 2, \dots, m$   $j \neq i$ , the resulting S-parameters are  $S_{i,j}=b_j$  for  $a_i=U_i$ . This allows for the reduction of large multicomponent  $n$ -port systems to a compact single component  $m$ -port ( $n \geq m$ ). The IFFT of the resulting  $m$ -port S-parameters produces the time domain impulse response  $S(t)$  which is useful for time domain analysis.

### 2.3 Time Domain Circuit Analysis

The time domain S-parameter circuit description for network analysis is given as<sup>6</sup>

$$b(t)=S(t)*a(t) \quad (2.18)$$

where  $*$  is the convolution operator. Note that  $S(t)$  is the system impulse response as described in section 2.1. Solving a linear system using 2.18 is computationally inefficient when compared to the frequency domain algorithm described in section 2.1.

## CHAPTER 3

## FREQUENCY DEPENDENT S-PARAMETER MODELS

This chapter reviews some of the S-parameter matrices representing two-port elements and derives the S-parameter matrices for coupled, multiconductor transmission lines commonly found in VLSI systems. The frequency dependent resistors, capacitors and inductors are modeled by two-port S-parameter matrices, while single and N coupled transmission lines are represented by two and 2N-port S-parameter matrices respectively. Coupled, multiconductor transmission lines are generated from parameters derived from two forms of analysis: frequency dependent quasi-TEM and fullwave analysis. The quasi-TEM dispersive model generates the S-parameter matrix from frequency dependent R,L,C,G parameters, while the fullwave analysis provides the frequency dependent propagation constants, characteristic impedance and the eigencurrent matrix needed to generate the non-TEM S-parameter representation.

## 3.1 Frequency Dependent R,L,C Element S-parameters

Resistors, capacitors and inductors can be represented by a 2x2 S-parameter matrix. For the normalized system given in Figure 3, the S-parameter matrix elements are given as<sup>7</sup>

$$S_{11}=S_{22}=Z/D \quad (3.1)$$

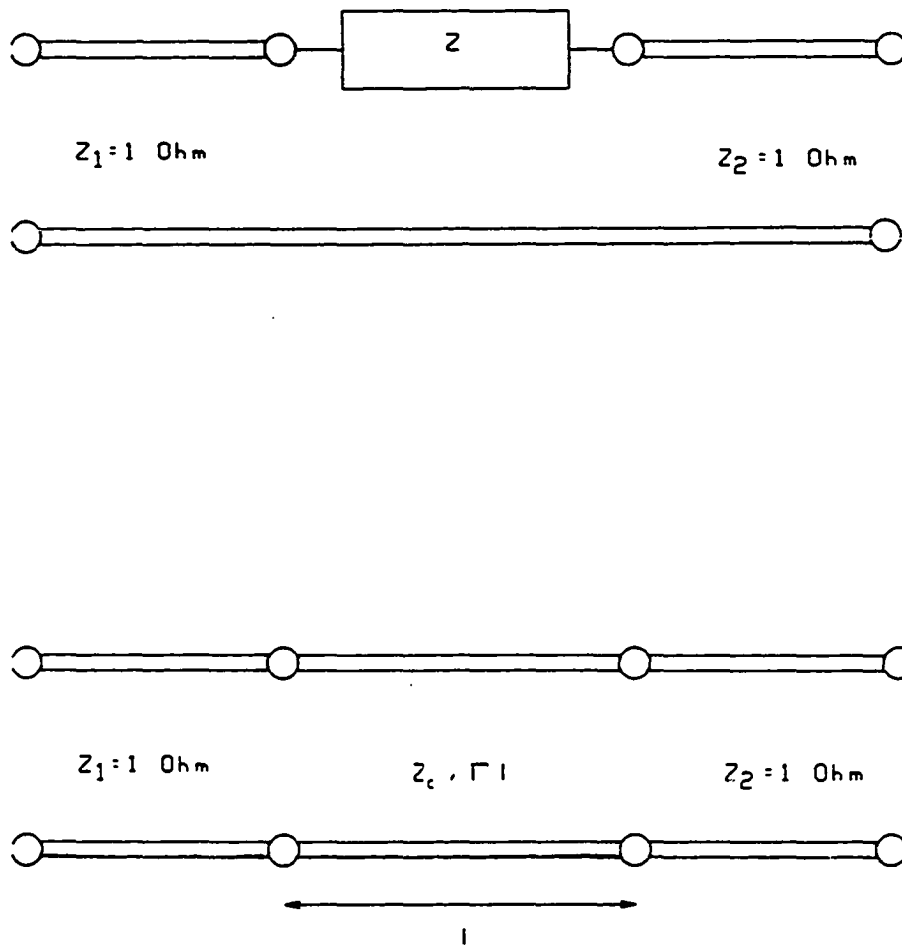


Figure 3. Two port S-parameter representation of an impedance and two port S-parameter representation of a transmission line of length  $l$ .

$$S_{12}=S_{21}=2/D \quad (3.2)$$

where

$$D=Z+2$$

$$Z=R(\omega) \quad \text{for a resistor}$$

$$Z=i\omega L(\omega) \quad \text{for an inductor}$$

$$Z=-i/[\omega C(\omega)] \quad \text{for a capacitor.}$$

### 3.2 Frequency Dependent Quasi-TEM Transmission Lines

The single transmission line can be represented by a two-port S-matrix. For the normalized system shown in Figure 3, the matrix elements are given as<sup>8</sup>

$$S_{11}=S_{22}=[Z_c^2-1]\sinh(\Gamma l) \quad (3.3)$$

$$S_{12}=S_{21}=2Z_c/D \quad (3.4)$$

where

$$D=2Z_c \cosh(\Gamma l) + [Z_c^2 + 1] \sinh(\Gamma l)$$

$$\Gamma = [(R(\omega) + i\omega L(\omega))(G(\omega) + i\omega C(\omega))]^{1/2}$$

$$Z_c = \frac{[R(\omega) + i\omega L(\omega)]^{1/2}}{[G(\omega) + i\omega C(\omega)]^{1/2}}$$

$R(\omega)$ —Resistance/meter

$G(\omega)$ —Conductance/meter

$L(\omega)$ —Inductance/meter

$C(\omega)$ —Capacitance/meter

$z$ —Line length (meter)

The S-parameters of the frequency dependent coupled lines are derived in the following manner. The frequency domain Telegraphist equations for a system of coupled lines of length  $l$  are<sup>9,10</sup>

$$\frac{dV(z)}{dz} = -ZI(z) \quad 0 < z < l \quad (3.4)$$

$$\frac{dI(z)}{dz} = -YV(z) \quad 0 < z < l \quad (3.5)$$

where  $Z=R(\omega)+i\omega L(\omega)$  and  $Y=G(\omega)+i\omega C(\omega)$ . From the frequency domain Telegraphist equation, one can derive the quasi-TEM wave equation

$$\frac{d^2V(z)}{dz^2} = -ZYV(z) \quad 0 < z < l \quad (3.6)$$

$$\frac{d^2I(z)}{dz^2} = -YZI(z) \quad 0 < z < l \quad (3.7)$$

For a  $z$  dependency of the voltage and currents proportional to

$$V(z) \propto V e^{\pm \Gamma z}$$

$$I(z) \propto I e^{\pm \Gamma z}$$

where  $\Gamma = \{\Gamma_1, \Gamma_2, \dots, \Gamma_N\}$  are the eigenmode propagation constants and  $V$  and  $I$  are constant voltage and current vectors respectively, the voltage wave equation reduces to the eigenvalue equation

$$([\Gamma]^2 - ZY)V = 0 \quad (3.8)$$

$$[\Gamma] = U\Gamma, \quad U = \text{Identity matrix}$$

from which the modal propagation eigenvalues  $\Gamma = \{\Gamma_1, \Gamma_2, \dots, \Gamma_N\}$  and corresponding voltage eigenvectors  $\Phi = \{V^1, V^2, \dots, V^N\}$  can be found. The conductor voltages and currents can be written in terms of forward (+) and reverse (-) traveling waves and expanded in terms of the eigenvectors<sup>11</sup>  $\Phi$ .

$$V_i(z) = V_i^- e^{\Gamma_i z} + V_i^+ e^{-\Gamma_i z} \quad i=1, 2, \dots, N \quad (3.9)$$

$$I_i(z) = I_i^- e^{\Gamma_i z} + I_i^+ e^{-\Gamma_i z} \quad i=1, 2, \dots, N \quad (3.10)$$

Expansion of the voltage vector  $V$  in terms of the eigenvectors  $\Phi$  gives

$$\begin{aligned} V(z) &= \Phi^1 (G_1^- e^{\Gamma_1 z} + G_1^+ e^{-\Gamma_1 z}) + \Phi^2 (G_2^- e^{\Gamma_2 z} + G_2^+ e^{-\Gamma_2 z}) + \dots + \Phi^N (G_N^- e^{\Gamma_N z} + G_N^+ e^{-\Gamma_N z}) \\ &= \Phi (G^- e^{\Gamma z} + G^+ e^{-\Gamma z}) \end{aligned} \quad (3.11)$$

where the  $G_i^+, G_i^-$ ,  $i=1,2,\dots,N$  are complex expansion coefficients representing the forward and reverse traveling components. Substituting the voltage eigenvector expansion into equation 3.4 results in an expression for the current  $I$

$$\begin{aligned} \frac{dV(z)}{dz} &= -ZI(z) \\ \rightarrow \Phi[\Gamma](G^-e^{\Gamma z} - G^+e^{-\Gamma z}) &= -ZI(z) \end{aligned} \quad (3.12)$$

$$\text{or } I(z) = Z^{-1}\Phi[\Gamma](-G^-e^{\Gamma z} + G^+e^{-\Gamma z}). \quad (3.13)$$

Comparing the forward and reverse components of the voltage and current expressions one finds that

$$V(z) = \Phi(G^+e^{-\Gamma z} + G^-e^{\Gamma z}) = \Phi(G^+(z) + G^-(z)) = V^+(z) + V^-(z) \quad (3.14)$$

$$I(z) = Z_c^{-1}\Phi(G^+e^{-\Gamma z} - G^-e^{\Gamma z}) = Z_c^{-1}\Phi(G^+(z) - G^-(z)) = I^+(z) + I^-(z) \quad (3.15)$$

where  $Z_c = \Phi[\Gamma]^{-1}\Phi^{-1}Z$  is defined as the characteristic impedance matrix of the coupled lines. Note that an identical set of equations can be derived in terms of a current eigenvector expansion.

The next step is applying boundary conditions. Referring to Figure 4, the terminations used to find the normalized scattering parameters are

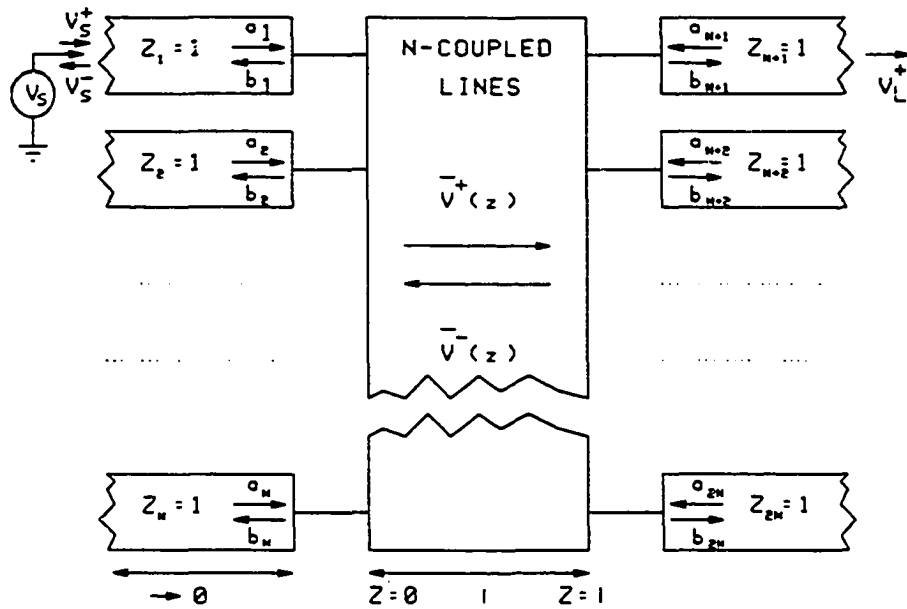


Figure 4. 2N port S-parameter representation of a N coupled transmission line.

decoupled one ohm transmission lines (or one ohm resistors). In terms of the source voltage vector  $V_s$ , the forward and reverse transmission line voltages can be written as

$$V^+(0) = \tau_s V_s + \rho_s V^-(0) \quad (3.16)$$

$$V^-(1) = \rho_L V^+(1) \quad (3.17)$$

where transmission and reflection coefficients for the normalized source and load are given by

$$\tau_s = Z_c (U + Z_c)^{-1}$$

$$\rho_s = (U - Z_c) (U + Z_c)^{-1}$$

$$\rho_L = (U - Z_c) (U + Z_c)^{-1}$$

and  $U$  is the identity matrix representing the 1 ohm decoupled load and source. Expanding equations 3.16 and 3.17 in terms of the eigenvector expansion coefficients,

$$\begin{aligned} V^+(0) &= \Phi G^+(0) = \tau_s V_s + \rho_s \Phi G^-(0) \\ \rightarrow G^+(0) &= \Phi^{-1} \tau_s V_s + \Phi^{-1} \rho_s \Phi G^-(0) \end{aligned} \quad (3.18)$$

$$\begin{aligned} V^-(1) &= \Phi G^-(1) = \rho_L \Phi G^+(1) \\ \rightarrow G^-(1) &= \Phi^{-1} \rho_L \Phi G^+(1). \end{aligned} \quad (3.19)$$

The voltages at the line ends  $z=0$  and  $z=1$  are related by

$$\begin{aligned} V^+(1) &= \Phi G^+(1) = \Phi [e^{\Gamma l}] G^+(0) \\ \rightarrow G^+(1) &= [e^{\Gamma l}] G^+(0) \end{aligned} \quad (3.20)$$

$$\begin{aligned} V^-(0) &= \Phi G^-(0) = \Phi [e^{\Gamma l}] G^-(1) \\ \rightarrow G^-(0) &= [e^{\Gamma l}] G^-(1) \end{aligned} \quad (3.21)$$

where the (diagonal) matrix  $[e^{\Gamma l}]$  represents the modal delay. With equations 3.20 and 3.21, equation 3.19 can be written as

$$G^-(0) = [e^{\Gamma l}] \Phi^{-1} \rho_L \Phi [e^{\Gamma l}] G^+(0). \quad (3.22)$$

By substitution of 3.22 into equation 3.18, one can solve for  $G^+(0)$

$$\begin{aligned} G^+(0) &= \Phi^{-1} \tau_s V_s + \Phi^{-1} \rho_s \Phi [e^{\Gamma l}] \Phi^{-1} \rho_L \Phi [e^{\Gamma l}] G^+(0) \\ \rightarrow G^+(0) &= \{ U - \Phi^{-1} \rho_s \Phi [e^{\Gamma l}] \Phi^{-1} \rho_L \Phi [e^{\Gamma l}] \}^{-1} \Phi^{-1} \tau_s V_s \end{aligned} \quad (3.23)$$

and combining equations 3.19 and 3.20 gives

$$G^-(1) = \Phi^{-1} \rho_L \Phi [e^{\Gamma l}] G^+(0). \quad (3.24)$$

The conductor voltages at the transmission line ends can now be found from equations 3.23 and 3.24,

$$V(0) = \Phi \{ G^+(0) + [e^{\Gamma l}] G^-(1) \} \quad (3.25)$$

$$V(1) = \Phi \{ [e^{\Gamma l}] G^+(0) + G^-(1) \}. \quad (3.26)$$

An eigenvector expansion for  $\omega=0$  if either the resistance or conductance matrix is zero can not be performed because the product of  $[Z]$  and  $[Y]$  produces a singular matrix. In the limit of  $\omega \rightarrow 0$ , the conductor voltages are given as

$R=G=0$  (Lossless lines)

$$V(0) = 0$$

$$V(1) = U$$

$R \neq 0, G=0$

$$V(0) = Rz \{ 2U + Rz \}^{-1}$$

$$V(1) = 2U \{ 2U + Rz \}^{-1}$$

$R=0, G \neq 0$

$$V(0) = -Gz \{ 2U + Gz \}^{-1}$$

$$V(1) = 2U \{ 2U + Gz \}^{-1}.$$

Where  $U$  is the identity matrix representing the normalized characteristic impedance matrix and  $z$  is the length of the transmission line segment.

The S-parameters for N coupled lines are the ratio of the voltage at the source and load terminations due to the excitation of a single line. It should be evident that due to the symmetry of the system only half of the ports need be calculated. For excitation of the  $i^{\text{th}}$  line with a source of 1 volt,

near end

$$S_{i,j} = V_j(0) \quad j=1,2,\dots,N \quad (3.27)$$

far end

$$S_{i,N+j} = V_j(1) \quad j=1,2,\dots,N \quad (3.28)$$

and from symmetry

$$S_{N+i,N+j} = S_{i,j} \quad j=1,2,\dots,N \quad (3.29)$$

$$S_{N+i,j} = S_{i,N+j} \quad j=1,2,\dots,N. \quad (3.30)$$

A  $2N \times 2N$  scatter matrix will be the result of ranging  $i$  over all  $N$  lines.

### 3.3 Frequency Dependent Non-TEM Transmission Lines

The propagation constants  $\Gamma$ , characteristic impedance  $Z_c$  and  $N \times N$  eigencurrent matrix  $\Psi$  can be found from the fullwave solution of  $N$  (plus ground) coupled, multiconductor transmission lines. The  $i_{km}$  components of the eigencurrent matrix, representing the current on line  $k$  for mode  $m$ , are defined as

$$i_{km} = \int J_{zkm} dx$$

where  $J_{zkm}$  is the  $z$  component of current density on line  $k$  for mode  $m$  and the integral is taken over the  $k_{th}$  line<sup>12</sup>. Once  $\Gamma, Z_c$  and  $\Psi$  are obtained, the voltage eigenvectors  $\Phi$  can be found and the  $S$ -parameter matrix can be obtained in the same fashion as described in Section 3.2.

The voltage eigenvectors are found from

$$\Phi = Z_c \Psi.$$

For the excitation of the  $i^{th}$  line with a source of 1 volt, the  $S$ -parameters are

$$\text{near end: } S_{i,j} = V_j(0) \quad j=1,2,\dots,N$$

$$\text{far end: } S_{i,N+j} = V_j(1) \quad j=1,2,\dots,N$$

and from symmetry

$$S_{N+i, N+j} = S_{i, j} \quad j=1, 2, \dots, N$$

$$S_{N+i, j} = S_{i, N+j} \quad j=1, 2, \dots, N$$

where for a line of length  $z=1$ , source and load located at  $z=0$  and  $z=1$  respectively and a source voltage vector  $V_s$

$$V(0) = \Phi \{ G^+(0) + [e^{\Gamma 1}] G^-(1) \}$$

$$V(1) = \Phi \{ [e^{\Gamma 1}] G^+(0) + G^-(1) \}$$

$$G^+(0) = \{ U - \Phi^{-1} \rho_s \Phi [e^{\Gamma 1}] \Phi^{-1} \rho_L \Phi [e^{\Gamma 1}] \}^{-1} \Phi^{-1} \tau_s V_s$$

$$G^-(1) = \Phi^{-1} \rho_L \Phi [e^{\Gamma 1}] G^+(0)$$

$$\tau_s = Z_c (U + Z_c)^{-1}$$

$$\rho_s = (U - Z_c) (U + Z_c)^{-1}$$

$$\rho_L = (U - Z_c) (U + Z_c)^{-1}$$

$U = 1$  ohm identity matrix.

Again, a  $2N \times 2N$  scatter matrix will be the result of ranging  $i$  over all  $N$  lines.

## CHAPTER 4

## NON-LINEAR TERMINATIONS

The analysis of frequency dependent systems with non-linear terminations must be done in both the frequency domain and the time domain. Non-linear terminations must be handled in the time domain, while frequency dependent effects must be dealt with in the frequency domain. This chapter describes an algorithm that allows for the simulation of non-linearly terminated frequency dependent systems. The algorithm proceeds as follows: First the frequency dependent S-parameters are calculated in such a manner as described in chapters 2,3 and 5. Next, the S-parameters are subjected to an impedance de-normalization (to minimize the time domain dispersion), then the S-parameters are transformed to their equivalent Y (admittance) parameters and Inverse Fast Fourier Transformed back to the time domain forming the Conductance Greens Function (CGF). Finally, once the time domain CGF has been obtained, the convolution integral along with standard circuit techniques can be used to calculate the time domain system response to an arbitrary source input with non-linear terminations.

## 4.1 Transforming S-parameters to Y-parameters

The impedance scaling of S-parameters is an important step in the procurement of the CGF because it allows for the selection of resistive

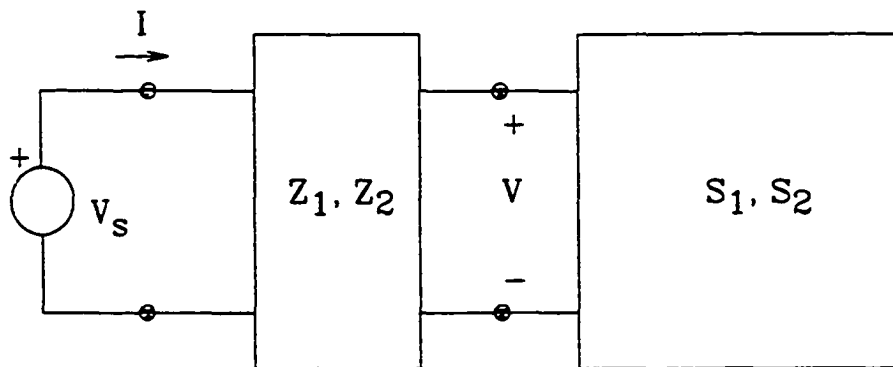


Figure 5. Network used for S-parameter impedance transformation and S-parameter to Y-parameter conversion.

terminations for a N-port system that minimizes the length of the time domain response. This is particularly important if the system S-parameters are normalized to unit terminations as described in chapters 2 and 3. The resulting time domain impulse response may be very long due to the large impedance mismatches. De-normalizing the S-parameters to a value close to the natural line impedances will minimize the length of the time domain response and significantly reduce the required calculation time. Referring to Figure 5, the incident and reflected voltages referenced to  $Z_1$  are<sup>13</sup>

$$2V_1^+ = V + Z_1 I = V_s \quad (4.1)$$

$$2V_1^- = V - Z_1 I. \quad (4.2)$$

The voltage S-parameter matrix referenced to  $Z_1$  is defined by

$$V_1^- = S_1 V_1^+. \quad (4.3)$$

Likewise, if the system were referenced to  $Z_2$  the resulting set of equations would be

$$2V_2^+ = V + Z_2 I = V_s \quad (4.4)$$

$$2V_2^- = V - Z_2 I \quad (4.5)$$

$$V_2^- = S_2 V_2^+. \quad (4.6)$$

The next step is to find the S-parameter matrix  $S_1$  given  $S_2$ ,  $Z_2$  and  $Z_1$  such that the port voltage  $V$  and current  $I$  remain unchanged between the two systems. Solving equations 4.4-4.6 for  $V$  and  $I$

$$V=(U+S_2)V_2^+ \quad (4.7)$$

$$I=Z_2^{-1}(U-S_2)V_2^+ \quad (4.8)$$

where  $U$ =Identity matrix

and inserting into equations 4.1 and 4.2,

$$2V_1^+=V+Z_1I=[(U+S_2)+Z_1Z_2^{-1}(U-S_2)]V_2^+ \quad (4.9)$$

$$2V_1^-=V-Z_1I=[(U+S_2)-Z_1Z_2^{-1}(U-S_2)]V_2^+. \quad (4.10)$$

Replacing  $V_1^-$  with  $V_1^+$  through equation 4.3 and equating equation 4.9 and 4.10 produces the desired transformation.

$$S_1=[(U+S_2)-Z_1Z_2^{-1}(U-S_2)][(U+S_2)+Z_1Z_2^{-1}(U-S_2)]^{-1} \quad (4.11)$$

To find the Y-parameters from S-parameters, one starts with the definition of admittance

$$YV=I \quad (4.12)$$

where using the notation of Figure 1

$$I = Z_1^{-1}(a-b) \quad (4.13)$$

$$V = Z_1^{-1}(a+b) \quad (4.14)$$

$$b = S_1 a \quad (4.15)$$

with  $Z_1$  the termination impedance. Keeping only the components entering and leaving the S-parameter network (which represent the components leaving and entering the termination elements respectively) reduces equations 4.13-4.15 to the following:

$$I = -Z_1^{-1}b \quad (4.16)$$

$$V = Z_1^{-1}a \quad (4.17)$$

$$b = S_1 a. \quad (4.18)$$

Substituting 4.16-4.18 into 4.12, eliminating  $a$  and solving for  $Y$  gives

$$Y = -Z_1^{-1}S_1Z_1^{-1}. \quad (4.19)$$

If the normalized S-parameters are calculated as defined in chapter 2 then equations 4.11 and 4.19 reduce to

$$S = [(U+S_n) - Z_o(U-S_n)] [(U+S_n) + Z_o(U-S_n)]^{-1} \quad (4.20)$$

$$Y = Z_o^{-1}SZ_o^{-1} \quad (4.21)$$

where  $S_n$  are the normalized S-parameters and  $Z_o$  the de-normalized termination Z-parameters.

#### 4.2 Y-parameter Time Domain Analysis

The time domain Y-parameters can be obtained by Inverse Fast Fourier Transforming the frequency domain Y-parameters calculated by equations 4.20-4.21

$$y(t) = \text{IFFT}(Y). \quad (4.22)$$

Here  $y(t)$  represents the Conductance Greens Function (CGF) of the frequency dependent system terminated in  $Z_o$ . The time domain response to an arbitrary input voltage  $v_i$  could be found by convoluting  $v_i$  with the CGF

$$i(t) = y(t) * v_i(t) = \int_0^t y(t-\tau) v_i(\tau) d\tau. \quad (4.23)$$

In order to allow for terminations other than  $Z_o$ , what is needed is a network analysis technique that will allow for the cancellation of the old termination  $Z_o$  and replace it with new nonlinear termination  $Z$ . Referring to Figure 6, an augmented network is created by inserting a

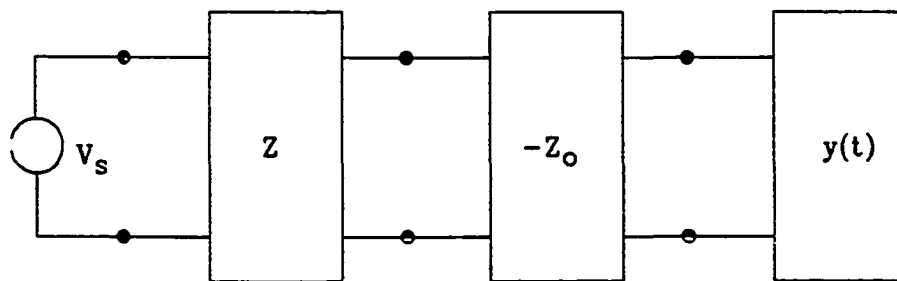


Figure 6. Augmented network used to cancel old termination  $Z_o$  and introduce nonlinear terminations  $Z$ .

negative impedance  $-Z_0$  between  $y(t)$  and the new termination  $Z$ . The negative impedance cancels out  $Z_0$ , effectively leaving only the desired nonlinear termination network  $Z^{14}$ .

## CHAPTER 5

## INCORPORATION OF EXTERNALLY GENERATED S-PARAMETERS

Externally incorporated S-parameters include measured and simulated data. This chapter describes how to make such data compatible with the techniques described in the previous chapters through sampling synchronization and impedance normalization.

## 5.1 Processing externally generated S-parameters

In order to make external data compatible with the techniques described in the previous Chapters, the data must be synchronized and impedance normalized.

Synchronize external data samples with the FFT sample rate. The FFT requires a uniform sample rate that is determined by the number of samples used and the period. If the data samples are not synchronized, then interpolation or curve fitting can be used.

The data must then be impedance normalized. Since data is rarely measured with a 1 ohm load, the data must be impedance scaled. The relationship between the desired normalized S-parameters  $S_n$  and the de-normalized S can be obtained from chapter 4 equation 4.17 by solving for  $S_n$

$$S_n = ((Z_o + U) + S(Z_o - U))^{-1} ((Z_o - U) + S(U + Z_o)) \quad (5.1)$$

where  $Z_0$  is the de-normalized termination impedance matrix which is normally diagonal for decoupled terminations, and  $U$  is the identity matrix.

Because the FFT requires both positive and negative frequency components the S-parameters for negative frequency components are required. If the system is passive, the negative frequency S-parameters are given by the complex conjugate of  $S$ ,

$$S(-\omega) = S^*(\omega). \quad (5.2)$$

It is unknown if equation 5.2 holds for the general case such as when a system contains active elements.

It should also be noted that when incorporating measured data, the termination impedance  $Z_0$  may be frequency dependent. In such a case, it would be necessary to include a frequency dependent file for the termination impedance along with the de-normalized S-parameters to obtain the correct normalized S-parameters.

An example of incorporating externally computed S-parameters for non-TEM coupled lines would proceed as follows. In the case of coupled, non-TEM structures where quasi-static or quasi-TEM dispersive R,L,C,G parameter extraction is insufficient, a fullwave analysis can be used to determine the propagation constants, characteristic impedance and eigencurrents of a coupled line<sup>15</sup>. A file of S-parameters (a macro) can

then be created from the propagation constants, characteristic impedance and eigencurrents (see Chapter 3). If the S-parameters are not normalized, they can be normalized through equation 5.1. The normalized S-parameters are now available to be used with other element models to evaluate the network response as described in Chapter 2.

## CHAPTER 6

## SPECTRAL COMPOSITION OF A PULSE

Calculating the spectrum of a pulse is useful because it gives the frequency, phase and amplitude of each spectral component of the signal. Such information can be useful in the design of transmission line networks and systems to ensure sufficient bandwidth for distortion free propagation. In this chapter, the trigonometric Fourier series of a general pulse is calculated, then Parseval's relation is used to calculate the integral-squared energy (or power) contents of a pulse composed of a finite number of terms. Finally the results are used to estimate the required system bandwidth for a pulse with a given period and rise-time.

## 6.1 Trigonometric Fourier Series of a General Pulse

The general trigonometric Fourier series expansion of a periodic function  $f(t)$  with period  $T$  such that  $f(t+T)=f(t)$  is<sup>16</sup>

$$f(t) = a_0 + \sum_{n=1}^{\infty} \{a_n \cos(2\pi n\omega_0) + b_n \sin(2\pi n\omega_0)\} \quad (6.1)$$

where  $\omega_0=2\pi/T$  is the fundamental frequency. By making use of the Fourier transform and its properties<sup>17</sup>, the Fourier series of a piece-wise linear function, and hence a general pulse, can be calculated with relative ease.

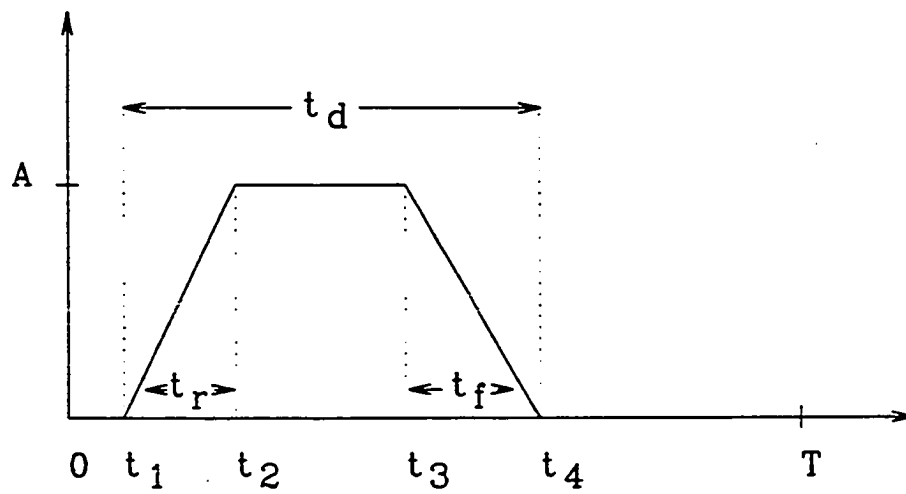


Figure 7. Waveform used for the derivation of the general Fourier series of a pulse.

Referring to Figure 7, the time domain expression describing the pulse can be written as

$$f(t) = \frac{A(t-\tau_1)}{\tau_2-\tau_1} u(t-\tau_1) - \frac{A(t-\tau_2)}{\tau_2-\tau_1} u(t-\tau_2) - \frac{A(t-\tau_3)}{\tau_4-\tau_3} u(t-\tau_3) + \frac{A(t-\tau_4)}{\tau_4-\tau_3} u(t-\tau_4) \quad (6.2)$$

where  $u(t-\tau) = 1$   $t \geq \tau$ ,  $0$   $t < \tau$  is the unit step function.

Differentiating equation 6.2 twice gives

$$f''(t) = \frac{A}{\tau_2-\tau_1} \delta(t-\tau_1) - \frac{A}{\tau_2-\tau_1} \delta(t-\tau_2) - \frac{A}{\tau_4-\tau_3} \delta(t-\tau_3) + \frac{A}{\tau_4-\tau_3} \delta(t-\tau_4) \quad (6.3)$$

where  $\delta(t-\tau)$  is a delta function.

Fourier transforming equation 6.3 and making use of the following properties of the Fourier transform

$$f''(t) \rightarrow (i\omega)^2 F(\omega)$$

$$f(t-\tau) \rightarrow F(\omega) e^{-i\tau\omega}$$

results in

$$F(\omega) = \frac{1}{\omega^2} \left\{ \frac{A}{\tau_2-\tau_1} e^{-i\tau_1\omega} - \frac{A}{\tau_2-\tau_1} e^{-i\tau_2\omega} - \frac{A}{\tau_4-\tau_3} e^{-i\tau_3\omega} + \frac{A}{\tau_4-\tau_3} e^{-i\tau_4\omega} \right\}. \quad (6.4)$$

To express the Fourier transform in terms of a Fourier series,

$$f(t) = \sum_{n=-\infty}^{\infty} F_n e^{in\omega_0 t}$$

substitute  $F_n \rightarrow \frac{F(\omega)}{T}$ ,  $\omega \rightarrow n\omega_0$  into equation 6.4 yielding

$$F_n = \frac{1}{T(n\omega_0)^2} \left\{ \frac{A}{\tau_2 - \tau_1} e^{-i\tau_1 n\omega_0} - \frac{A}{\tau_2 - \tau_1} e^{-i\tau_2 n\omega_0} - \frac{A}{\tau_4 - \tau_3} e^{-i\tau_3 n\omega_0} + \frac{A}{\tau_4 - \tau_3} e^{-i\tau_4 n\omega_0} \right\}. \quad (6.5)$$

Finally, the trigonometric expansion coefficients  $a_n$  and  $b_n$  of equation 6.1 are found by separating the real and imaginary components of  $F_n$

$$a_0 = F_0$$

$$a_n = 2\text{Re}(F_n)$$

$$b_n = -2\text{Im}(F_n).$$

or,

$$a_0 = A \left\{ \frac{\tau_2 - \tau_1}{2} + (\tau_3 - \tau_2) + \frac{\tau_4 - \tau_3}{2} \right\} \quad (6.6)$$

$$a_n = \frac{2A}{T(n\omega_0)^2} \left[ \frac{1}{\tau_2 - \tau_1} \{ \cos(\tau_1 n\omega_0) - \cos(\tau_2 n\omega_0) \} - \frac{1}{\tau_4 - \tau_3} \{ \cos(\tau_3 n\omega_0) - \cos(\tau_4 n\omega_0) \} \right] \quad (6.7)$$

$$b_n = \frac{2A}{T(n\omega_0)^2} \left[ \frac{1}{\tau_2 - \tau_1} \{ \sin(\tau_1 n\omega_0) - \sin(\tau_2 n\omega_0) \} - \frac{1}{\tau_4 - \tau_3} \{ \sin(\tau_3 n\omega_0) - \sin(\tau_4 n\omega_0) \} \right]. \quad (6.8)$$

## 6.2 Integral-Squared Error of a Pulse

The energy or power in a pulse can be represented either in the frequency domain or in the time domain through Parseval's theorem<sup>18,19</sup>. The theorem states that if a function  $f(t)$  is represented by a complete, (over the interval  $\{t_1, t_2\}$ ) orthogonal set  $T_n(t)$

$$f(t) = \sum_{n=1}^{\infty} f_n T_n(t), \quad (6.9)$$

then its integral-squared value is given by

$$\int_{t_1}^{t_2} |f(t)|^2 dt = \sum_{n=1}^{\infty} |f_n|^2 K_n \quad (6.10)$$

where  $K_n = \langle T_n(t), T_n(t) \rangle$  is the inner product of  $T_n(t)$ . Parseval's relation for the trigonometric Fourier series is

$$\frac{1}{T} \int_0^T |f(t)|^2 dt = a_0^2 + \frac{1}{2} \sum_{n=1}^{\infty} (a_n^2 + b_n^2). \quad (6.11)$$

When the series is truncated at a finite  $N$ , the resulting integral-squared error of the orthogonal series approximation to  $f(t)$  over the interval  $(0, T)$  is given by

$$\int_0^T |\epsilon_N(t)|^2 dt = \frac{1}{T} \int_0^T |f(t)|^2 dt - \left[ a_0^2 + \frac{1}{2} \sum_{n=1}^N (a_n^2 + b_n^2) \right]. \quad (6.12)$$

The coefficients  $a_n$  and  $b_n$  have been calculated in equations 6.6-6.8. The time domain integral can be found by directly integrating equation 6.2,

$$\begin{aligned} \frac{1}{T} \int_0^T |f(t)|^2 dt &= \frac{T^3 - \tau_1^3}{3T(\tau_2 - \tau_1)^2} - \frac{\tau_1(T^2 - \tau_1^2)}{T(\tau_2 - \tau_1)^2} + \frac{\tau_1^2(T - \tau_1)}{T(\tau_2 - \tau_1)^2} \\ &- \frac{(T^3 - \tau_2^3)}{3T(\tau_2 - \tau_1)^2} + \frac{\tau_1(T^2 - \tau_2^2)}{T(\tau_2 - \tau_1)^2} + \frac{(\tau_2^2 - 2\tau_1\tau_2)(T - \tau_2)}{T(\tau_2 - \tau_1)^2} \end{aligned}$$

$$\begin{aligned}
& + \frac{(T^3 - \tau_3^3)}{3T(\tau_4 - \tau_3)^2} - \left\{ \frac{\tau_3}{T(\tau_4 - \tau_3)^2} + \frac{\tau_2 - \tau_1}{T(\tau_2 - \tau_1)(\tau_4 - \tau_3)} \right\} (T^2 - \tau_3^2) \\
& + \left\{ \frac{\tau_3^2}{T(\tau_4 - \tau_3)^2} + \frac{2(\tau_2\tau_3 - \tau_1\tau_3)}{T(\tau_2 - \tau_1)(\tau_4 - \tau_3)} \right\} (T - \tau_3) - \frac{(T^3 - \tau_4^3)}{3T(\tau_4 - \tau_3)^2} \\
& + \left\{ \frac{\tau_3}{T(\tau_4 - \tau_3)^2} + \frac{\tau_2 - \tau_1}{T(\tau_2 - \tau_1)(\tau_4 - \tau_3)} \right\} (T^2 - \tau_4^2) \\
& + \left\{ \frac{\tau_4^2 - 2\tau_3\tau_4}{T(\tau_4 - \tau_3)^2} + \frac{2(\tau_4\tau_1 - \tau_4\tau_2)}{T(\tau_2 - \tau_1)(\tau_4 - \tau_3)} \right\} (T - \tau_4). \tag{6.13}
\end{aligned}$$

### 6.3 Estimation of Pulse Spectrum and Required System Bandwidth

With equations 6.6-6.8, 6.12 and 6.13 an estimation of the pulse spectrum or required system bandwidth can be made as a function of the period, duty cycle, rise time and fall time. Referring to Figure 7, the period (T) is the reciprocal of the clock frequency, the duty cycle ( $\tau_D/T$ ) represents the fraction of the period where the pulse is non-zero, and  $\tau_r$ ,  $\tau_f$  are the rise time and fall times of the pulse respectively. Figure 8 shows a plot of the number of required Fourier terms as a function of percent rise and fall times for a 50% duty cycle pulse with an integral-squared error (ISE) of 1%, 0.5% and 0.1%. Note that as the rise and fall times decrease, the number of Fourier terms required to form the pulse

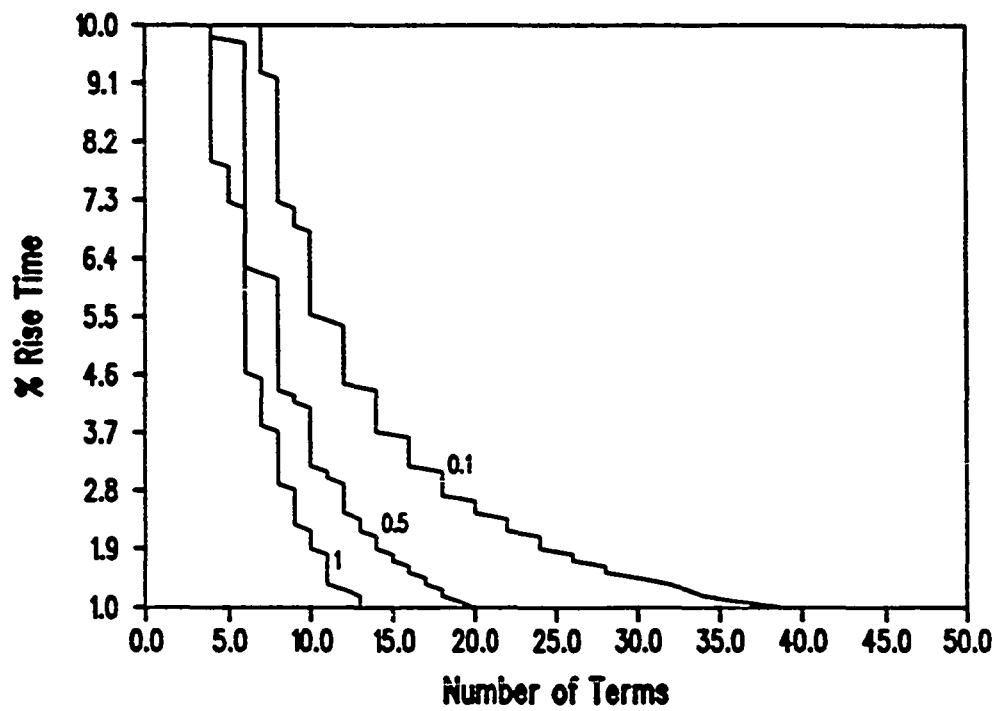


Figure 8. Number of fourier terms as a function of percent rise time and fall time for a 50% duty cycle and 1%, 0.5% and 0.1% integral-squared error.

with a 1% ISE increases. As an example of using Figure 8 to determine the spectrum of a clocked pulse, a pulse train with a 50% duty cycle and a 100 mhz clock rate will have a 4x100 mhz spectrum for a 10% rise and fall times because 4 terms are needed to maintain a 1% ISE, while maintaining the same clock rate, a pulse with 1% rise and fall times will have a 1200 mhz spectrum. A plot of the pulse with 10% rise and fall times using four fourier terms for a 1% ISE and 7 fourier terms for an 0.1% ISE is shown in Figure 9. Decreasing the integral-squared error to 0.1% produces, as expected, a better fit. From an engineering standpoint, the ISE bound should probably fall between 1% and 0.1%.

A practical consequence of knowing the spectral bandwidth of the pulse train is that it defines the required upper bound of the system bandwidth for a transmission line. Referring to Figure 10, the system bandwidth, for most practical purposes, can be defined as the beginning of the frequency range at which on average the magnitude of the ratio of the signal at the load to the signal at the load is down by a factor of two (3 db) from its average lower frequency ratio. The 3 db frequency ( $f_{3db}$ ) represents the cutoff frequency where frequencies below  $f_{3db}$  belong to the system pass band and on average are only mildly attenuated in magnitude and non-linearly shifted in phase. Frequencies above belong to the system stop band and can be severely attenuated and phase shifted. For minimal signal transmission distortion, the spectral bandwidth of the pulse train must fit well within the transmission line pass band, if not, spectral components above  $f_{3db}$  will be affected and the resulting time domain signal will be distorted.

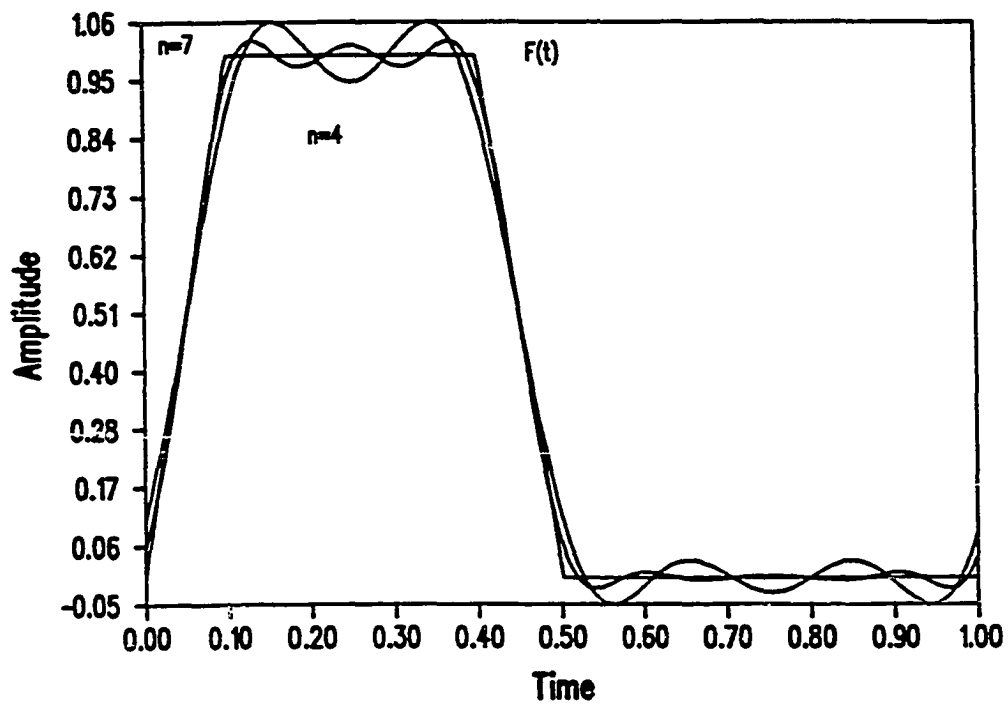


Figure 9. Plot of 10% rise and fall time pulse with four and seven term approximation corresponding to 1% and 0.1% integral-squared error.

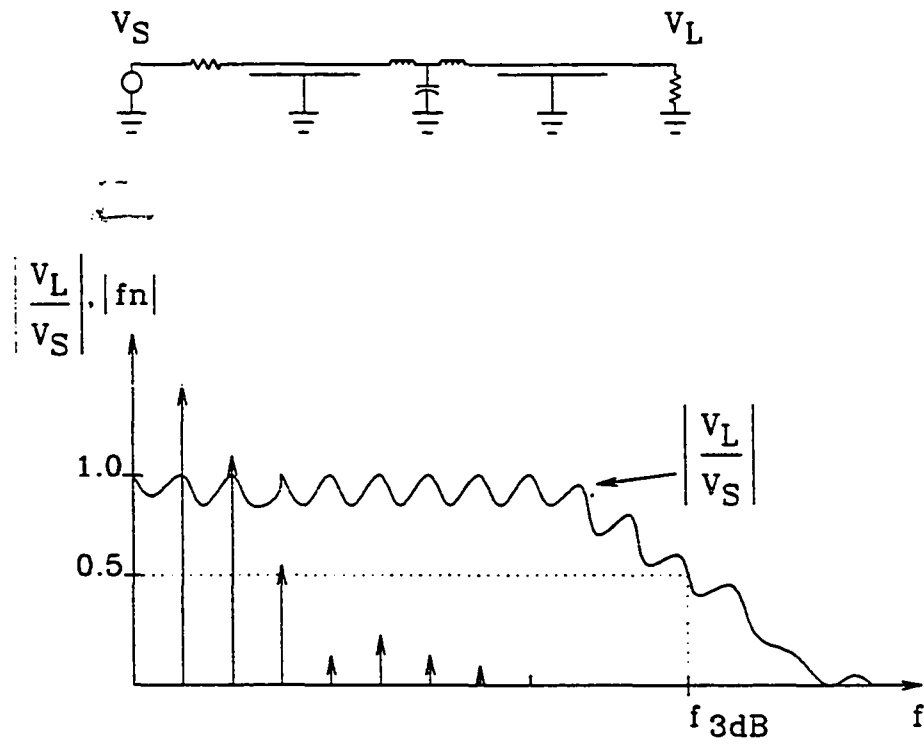


Figure 10. A transmission line network and system transfer function.

## CHAPTER 7

## S-PARAMETER ANALYSIS OF INTERCONNECT DISCONTINUITIES

S-parameter analysis of VLSI interconnect discontinuities can be conducted in an exact manner with a full wave analysis, or in terms of some form of an approximation. Full wave analysis methods tend to be cumbersome to implement and time consuming to execute. Hence, emphasis tends to be placed on techniques that approximate the effects of discontinuities. For most engineering purposes the effects of VLSI discontinuities can, to first order, be accounted for by RLC networks. In this chapter, Poynting's theorem is used to provide an argument for the validity of approximating discontinuities with RLC networks. Discrete component networks describing VLSI discontinuities are presented in S-parameter format and discussed.

## 7.1 Poynting's Theorem

Poynting's theorem<sup>20</sup> is a statement of conservation of energy. For a continuous distribution of charge and current, the total rate of work done by the fields in a finite volume  $V$  is

$$\int_V \mathbf{J} \cdot \mathbf{E} d^3x = \frac{1}{4\pi} \int_V [c \nabla \cdot (\mathbf{E} \times \mathbf{H}) + \mathbf{E} \cdot \frac{\partial \mathbf{D}}{\partial t} + \mathbf{H} \cdot \frac{\partial \mathbf{B}}{\partial t}] d^3x \quad (7.1)$$

where  $\mathbf{J}$  is the current density,  $\mathbf{E}$  is the electric field,  $\mathbf{D}$  is the electric displacement,  $\mathbf{B}$  is the magnetic flux density,  $\mathbf{H}$  is the magnetic field and  $c$  is the speed of light. Assuming the fields and sources have a harmonic time dependence of  $e^{-i\omega t}$ , Poynting's theorem becomes

$$\frac{1}{2} \int_{\mathbf{v}} \mathbf{J}^* \cdot \mathbf{E} d^3\mathbf{x} - \frac{c}{8\pi} \int_{\mathbf{v}} [-\nabla \cdot (\mathbf{E} \times \mathbf{H}^*) - \frac{\omega}{c} (\mathbf{E} \cdot \mathbf{D}^* - \mathbf{B} \cdot \mathbf{H}^*)] d^3\mathbf{x}, \quad (7.2)$$

where  $*$  implies complex conjugate. Now define

$$\mathbf{S} = \frac{c}{8\pi} (\mathbf{E} \times \mathbf{H}^*) \quad (7.3)$$

$$w_e = \frac{1}{16\pi} (\mathbf{E} \cdot \mathbf{D}^*) \quad (7.4)$$

$$w_m = \frac{1}{16\pi} (\mathbf{B} \cdot \mathbf{H}^*) \quad (7.5)$$

where  $w_e$  and  $w_m$  are respectively the electric and magnetic densities and  $\mathbf{S}$  is the complex pointing vector. Equation 7.2 can now be written as

$$\frac{1}{2} \int_V \mathbf{J}^* \cdot \mathbf{E} d^3x + 2i\omega \int_V (w_e - w_m) d^3x + \oint_S \mathbf{S} \cdot \mathbf{n} da = 0 \quad (7.6)$$

where the divergence theorem has been used to create a surface integral from the volume integral.

Equation 7.6 is a complex equation whose real and imaginary components represent power transfer/loss and reactive/stored energy respectively. The real components, given by equation 7.7, show that the steady-state time-average rate of power loss within the volume  $V$  is equal to the difference in the average flow of power into and out of the volume through the bounding surface  $S$ . The imaginary components, given by equation 7.8, represent reactive or stored energy.

$$\frac{1}{2} \int_V \operatorname{Re}(\mathbf{J}^* \cdot \mathbf{E}) d^3x + 2\omega \int_V \operatorname{Im}(w_e - w_m) d^3x + \oint_S \operatorname{Re}(\mathbf{S} \cdot \mathbf{n}) da = 0 \quad (7.7)$$

$$\frac{1}{2} \int_V \operatorname{Im}(\mathbf{J}^* \cdot \mathbf{E}) d^3x + 2\omega \int_V \operatorname{Re}(w_e - w_m) d^3x + \oint_S \operatorname{Im}(\mathbf{S} \cdot \mathbf{n}) da = 0 \quad (7.8)$$

## 7.2 Application of Poynting's Theorem to a Discontinuity.

The complex Poynting's theorem can now be used to describe the effects of a general transmission line discontinuity. Figure 11 shows a discontinuity region defined by a volume  $V$  and bounded by a surface  $S$  between two transmission line segments  $T_1$  and  $T_2$ . Such a region may represent a bend or a via in a stripline. Assuming that the desired power flow is from  $T_1$  to  $T_2$  through the surfaces  $S_1$  to  $S_2$  then, according to Poynting's theorem, the effects of the discontinuity can be represented as

$$\int_{S_1} \Phi \mathbf{S} \cdot \mathbf{n} da - \int_{S_2} \Phi \mathbf{S} \cdot \mathbf{n} da = \frac{1}{2} \int_V \mathbf{J}^* \cdot \mathbf{E} d^3x + 2i\omega \int_V (w_e - w_m) d^3x + \int_{S_3} \Phi \mathbf{S} \cdot \mathbf{n} da \quad (7.9)$$

where  $S_3$  is the remaining surface integral. If the power entering at  $S_1$  is represented as the product of a voltage and current ( $\frac{1}{2}V^*I$ ), then the resistive and reactive components of the input impedance ( $Z=R+iX$ ), seen at  $S_1$ , are

$$R = \frac{1}{|I|^2} \left\{ \frac{1}{2} \int_V \text{Re}(\mathbf{J}^* \cdot \mathbf{E}) d^3x + 2\omega \int_V \text{Im}(w_e - w_m) d^3x + \int_{S_2} \text{Re}(\mathbf{S} \cdot \mathbf{n}) da + \int_{S_3} \text{Re}(\mathbf{S} \cdot \mathbf{n}) da \right\} \quad (7.10)$$

$$X = \frac{1}{|I|^2} \left\{ \frac{1}{2} \int_V \text{Im}(\mathbf{J}^* \cdot \mathbf{E}) d^3x + 2\omega \int_V \text{Re}(w_e - w_m) d^3x + \int_{S_2} \text{Im}(\mathbf{S} \cdot \mathbf{n}) da + \int_{S_3} \text{Im}(\mathbf{S} \cdot \mathbf{n}) da \right\}. \quad (7.11)$$

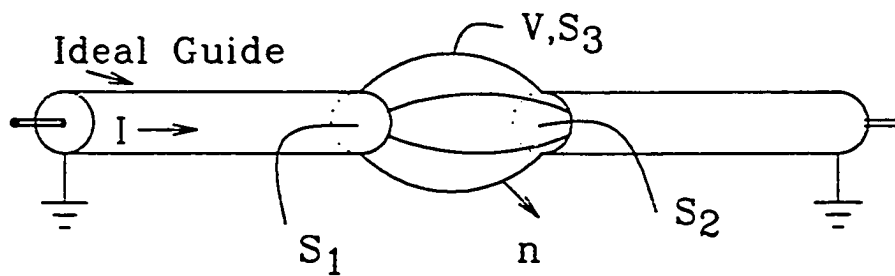


Figure 11. A discontinuity region defined by a the volume  $V$  and bounded by the surface  $S$  between two transmission line segments  $T_1$  and  $T_2$ .

An explanation of the terms are as follows. The real component of the volume integral of  $\mathbf{J}^* \cdot \mathbf{I}$  represents work done by the fields in the volume  $V$ , while the imaginary term represents the reactive effects. An example of the  $\mathbf{J}^* \cdot \mathbf{I}$  term would be that of a resistor. The real component would describe resistive heating due to ohmic losses and the imaginary component the effects of the distributed inductance and capacitance of the resistor. The real component of the  $w_m - w_e$  volume is purely reactive in nature. If the electric term  $w_e$  dominates the integral, the reactance seen at  $S_1$  is capacitive. If the magnetic term  $w_m$  dominates the integral, the reactance is inductive. Evanescent (non-propagating) fields due to a discontinuity give rise to such a frequency dependent reactance. A lossy dielectric within the volume will give rise to power dissipation that is given by the negative component of the  $w_m - w_e$  integral. A non-zero real component of the  $S_3$  surface integral would represent escaping radiation (if the surface is taken to infinity) which can be induced by a discontinuity in the form of high frequency components. The imaginary component represents fluctuating fields through the surface  $S_3$ .

If escaping radiation due to the discontinuity is neglected and a lossless discontinuity is assumed, equations 7.10-7.11 reduce to (with the impedance of  $T_2$  subtracted out)

$$R \approx \frac{1}{|I|^2} \left\{ \frac{1}{2} \int_{\mathcal{V}} \mathbf{J}^* \cdot \mathbf{E} d^3\mathbf{x} \right\} = \frac{1}{|I|^2} \left\{ \frac{1}{2} \int_{\mathcal{V}} \sigma |\mathbf{E}|^2 d^3\mathbf{x} \right\} \quad (7.12)$$

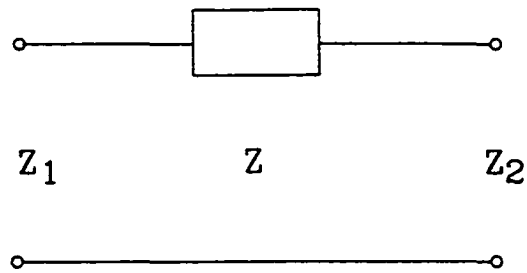
$$X \approx \frac{1}{|I|^2} \left\{ 2\omega \int_{\mathcal{V}} (w_m - w_e) d^3\mathbf{x} \right\} \quad (7.13)$$

where  $\sigma$  is the real conductivity. Equations 7.12 and 7.13 suggest, that to first order, the resistive and reactive effects of discontinuities can be approximated by an RLC network. While not discussed here, algorithms that extract the effective C, L and R parameters are available in the literature<sup>21,22</sup>.

### 7.3 S-parameter Network Models of Interconnect Discontinuities

Figure's 12-15 show the S-parameter networks and matrices for series impedance, shunt admittance, T-network and Pi-network respectively<sup>23</sup>. Note that the impedance and admittance elements represent networks of point source RLC elements. As an example, Figure 16 shows a T-network used to model a VLSI bend or via. For this case,  $Z_1=Z_3=R/2+i\omega L/2$  and  $Z_2=1/i\omega C$ . Other models can be found in the literature<sup>24</sup>.

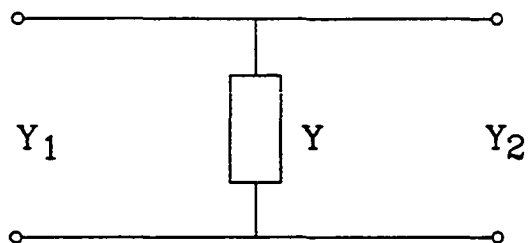
An important engineering question arises concerning itself as to when the lumped elements representing the effects of the discontinuity can be neglected. From Figures 12-15, the effects of the elements are minimized when  $S_{11}=S_{22} \rightarrow 0$ ,  $S_{12}=S_{21} \rightarrow 1$  and if the characteristic impedances of port 1 and 2 are equal. If the characteristic impedances are



$$S = \frac{1}{D_S} \begin{bmatrix} Z + Z_2 - Z_1 & 2\sqrt{Z_1 Z_2} \\ 2\sqrt{Z_1 Z_2} & Z + Z_1 - Z_2 \end{bmatrix}$$

where:  $D_S = Z + Z_1 + Z_2$

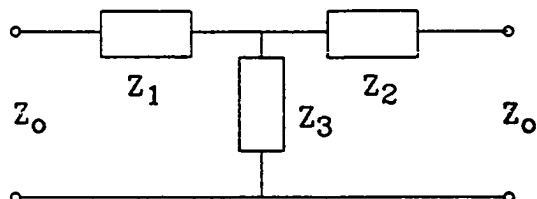
Figure 12. Series impedance S-parameters.



$$S = \frac{1}{D_s} \begin{bmatrix} Y_1 - Y_2 - Y & 2\sqrt{Y_1 Y_2} \\ 2\sqrt{Y_1 Y_2} & Y_2 - Y_1 - Y \end{bmatrix}$$

where:  $D_s = Y + Y_1 + Y_2$

Figure 13. Shunt admittance S-parameters.



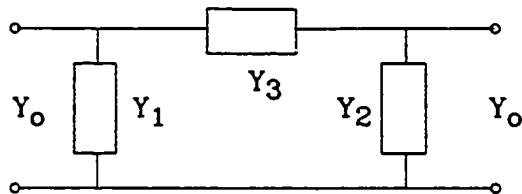
$$S = \frac{1}{D_S} \begin{bmatrix} -Z_0^2 + PZ_0 + D & 2Z_0Z_3 \\ 2Z_0Z_3 & -Z_0^2 - PZ_0 + D \end{bmatrix}$$

$$\text{where: } D_S = Z_0^2 + (Z_1 + Z_2 + 2Z_3)Z_0 + D$$

$$D = Z_1Z_2 + Z_2Z_3 + Z_3Z_1$$

$$P = Z_1 - Z_2$$

Figure 14. T-network S-parameters.



$$S = \frac{1}{D_s} \begin{bmatrix} Y_o^2 - PY_o - D & 2Y_oY_3 \\ 2Y_oY_3 & Y_o^2 + PY_o - D \end{bmatrix}$$

$$\text{where: } D_s = Y_o^2 + (Y_1 + Y_2 + 2Y_3)Y_o + D$$

$$D = Y_1Y_2 + Y_2Y_3 + Y_3Y_1$$

$$P = Y_1 - Y_2$$

Figure 15. Pi-network S-parameters.

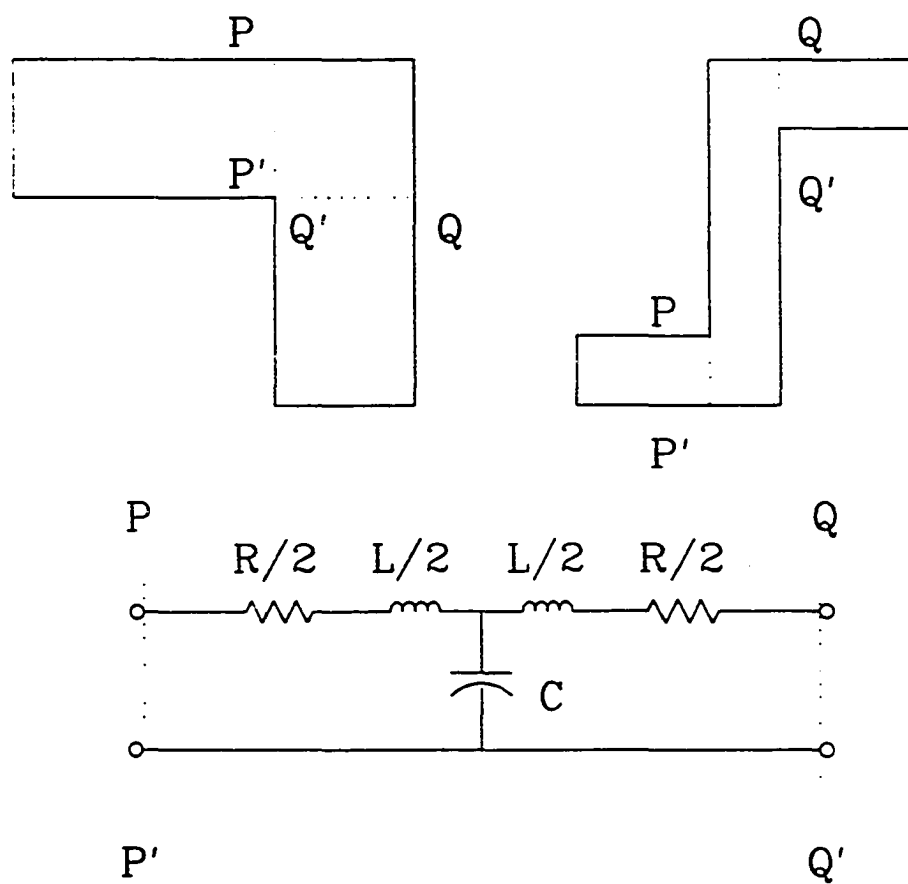


Figure 16. Equivalent T-network circuit of a bend and via.

mismatched, then the discontinuity can be neglected if the magnitude of the mismatch is much larger than the magnitude of the impedance of the lumped element. An example of a potentially mismatched discontinuity is the via. Since the via is predominantly inductive in nature, a series impedance, as shown in Figure 12, can be used to model the discontinuity. To determine if the effects of the discontinuity can be neglected, evaluate  $Z=i\omega L$  at the highest significant spectral component expected in the incident waveform (see Chapter 6). If  $Z \ll (Z_2-Z_1)$  then the effects of the via discontinuity can be neglected. In the case of no mismatch, the via can be neglected if  $Z \ll (Z_2+Z_1)$ .

## CHAPTER 8

### IMPLEMENTATION OF THE S-PARAMETER ANALYSIS TECHNIQUE

This chapter describes the computer implementation of the S-parameter algorithms introduced in the preceding chapters. First, an overall system overview is given describing, in general, how the algorithm functions. This is followed by a description of the system architecture and the numerical techniques applied. Finally, the last section examines the potential simulation error that can be introduced by Fourier aliasing and describes how aliasing can be detected and prevented.

#### 8.1 System Overview

The architecture of the implemented algorithm is shown in Figure 17. The time domain and frequency domain are linked by a Fast Fourier and Inverse Fast Fourier Transform (FFT/IFFT). A typical analysis would proceed as follows. First, a periodic input waveform is defined in the time domain with the Time Base Generator. Then, an FFT is automatically performed to go into the frequency domain where a graphically based Network Editor is used to create a file or recall and edit an existing file. The Network Editor makes use of predefined network elements whose parameters are user defined with the Library Editor and stored in the Data Base. Finally, the network is solved using the technique described in chapter 2 and results are graphically displayed in the frequency domain

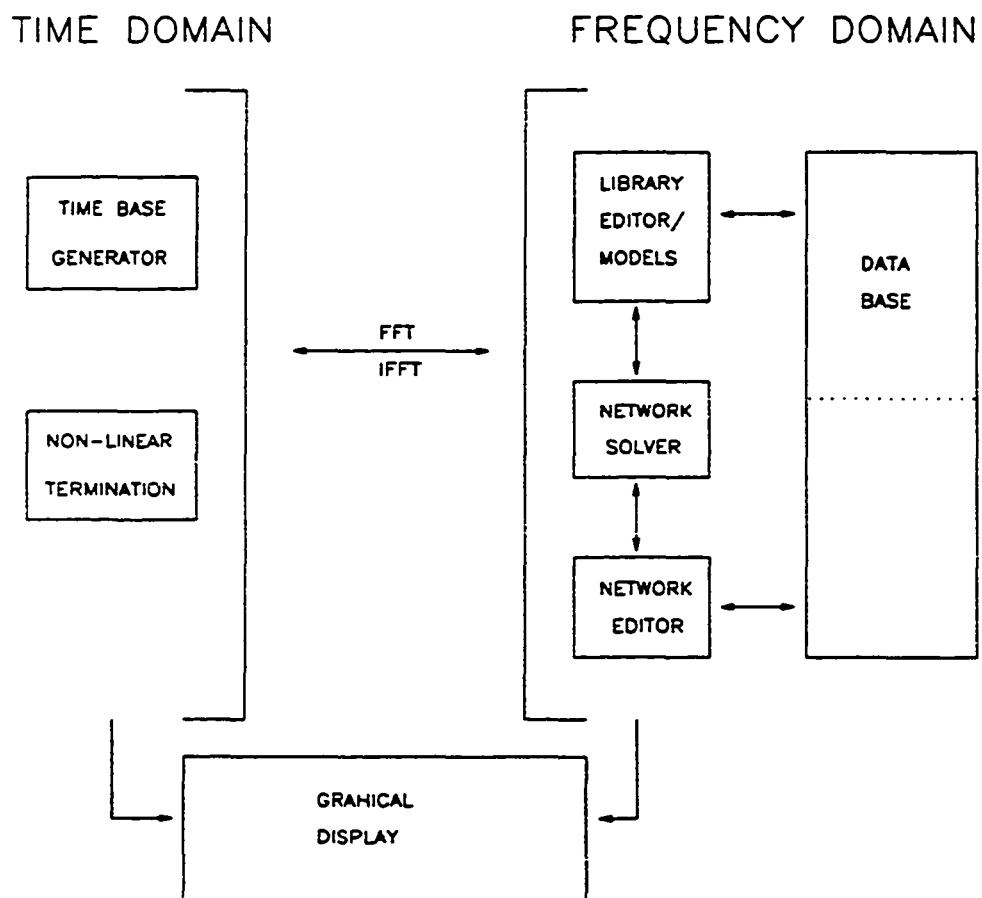


Figure 17. Architecture of the implemented algorithm.

or, through an IFFT, in the time domain. If the network is to be solved with non-linear terminations, the time domain CGF impulse response is calculated for the linear component of the system, the non-linear terminations are selected using the Non-Linear Termination Editor, and the time domain response is calculated through use of a convolution integral.

## 8.2 Architecture

The system employs a modular architecture which provides for a flexible and adaptable system. Each module ties into the overall system through a predefined I/O system, allowing for easy upgrading or changing of modules, when for example, a new editor configuration, numerical technique, or implementation of new library model is required. A brief description of the modules follow.

### FREQUENCY DOMAIN

LIBRARY EDITOR/MODELS: When a network is simulated, the index of a given network element is passed to the library, which then returns S-parameters generated by the model (and data base parameters) corresponding to that element's index. The editor is used to define the parameters (which can be frequency dependent) stored in the data base and used by the library models which include resistors, capacitors, inductors,

and lossy coupled lines. The library also contains file information of user supplied macros, measured data, or computer simulated S-parameters.

**NETWORK EDITOR:** This module is used to create, edit and file (save/recall) networks that are to be simulated.

**NETWORK SOLVER:** The network solver is the "number cruncher" component of the system where a linear system of equations is solved.

#### TIME DOMAIN

**TIME BASE GENERATOR:** The time base generator provides a means for which a user can generate any time domain periodic waveform desired such as pulses, exponential, noise, clipped signals etc..

**NON-LINEAR TERMINATION:** Contains models of the non-linear elements which would include BJT, MOS, and FET devices.

### 8.3 Numerical Techniques

This section describes the implemented numerical techniques.

LINEAR ALGEBRAIC EQUATIONS: LU decomposition is used for solving or inverting a system of linear equations. The algorithm was taken from Numerical Recipes<sup>25</sup> and modified for complex arithmetic.

EIGENVECTORS AND EIGENVALUES OF A GENERAL COMPLEX MATRIX:

The general (asymmetric) complex eigensystem is solved by first reducing the general matrix to an upper Hessenberg form by unitary similarity transformations and then applying the QR method extracting the eigenvectors and eigenvalues. The algorithms are translated and adapted from the MATLAB<sup>26</sup> routines.

#### 8.4 Fourier Aliasing (Error Analysis)

The S-parameter frequency domain equations used in SPTLA are exactly solved by Fourier transform methods. Hence, in the frequency domain, simulation error is limited to the numerical algorithms implemented and the inherent accuracy of the computer. However, potential error can be introduced when a time domain continuous-time signal is discretized (represented by a discrete-time set of points) and fast Fourier transformed to the frequency domain. If an insufficient number of discrete-time points are fast Fourier transformed, a phenomena known as

frequency aliasing occurs resulting in simulation error. This section explains how to detect and prevent aliasing.

When a time domain signal is generated with the program, the user is approximating a periodic, continuous-time function  $f(t)$  with a discrete-time function

$$f(t) \approx f_n(\delta n) \quad n=0,1,2,3\dots N$$

where  $\delta$  is the sampling interval. Since  $f(t)$  is periodic over  $T$

$$f(T+t) = f(t) \approx f_n(\tau n) \quad n=0,1,2,3\dots N,$$

then the function need only be sampled over the interval  $T$  with a sampling interval of

$$\delta = T/N.$$

The reciprocal of  $\delta$  is called the sampling rate and has the unit of samples per time.

For the sampling interval  $\delta$ , there is a special corresponding frequency,  $f_c$ , called the Nyquist<sup>27</sup> critical frequency which is given as

$$f_c = 1/2\delta.$$

If a bandwidth limited signal contains frequency components up to but not exceeding  $f_c$ , then Nyquist's relation requires a sampling rate of  $2f_c$  to preserve signal integrity. The total number of samples over a period  $T$  can then be written as

$$N = 2Tf_c.$$

Unfortunately, most electronic signals used for digital circuits are not band limited and actually have an infinite bandwidth. When a signal is under sampled, that is if the Nyquist criterion is violated and the signal contains spectral components greater than  $f_c$ , then a phenomena known as aliasing occurs. Spectral components greater than  $f_c$  are folded back into lower frequency components below  $f_c$  (hence the term aliasing) introducing an error into the representation of  $f(t)$ . Fortunately, for all practical signals used in digital circuits, the magnitude of the spectrum  $F_n$  uniformly decreases at higher frequencies. Most of the energy is carried by components lying within a well defined frequency interval, and the error introduced by ignoring the high frequency tail can be neglected. Hence, at some frequency the signal is for all practical purposes band limited and can be sampled at a finite  $N$ . Figure 18 illustrates the effects of aliasing. The top figure shows the spectrum of a signal that was correctly sampled at a rate greater than  $2f_c$ , while the bottom figure

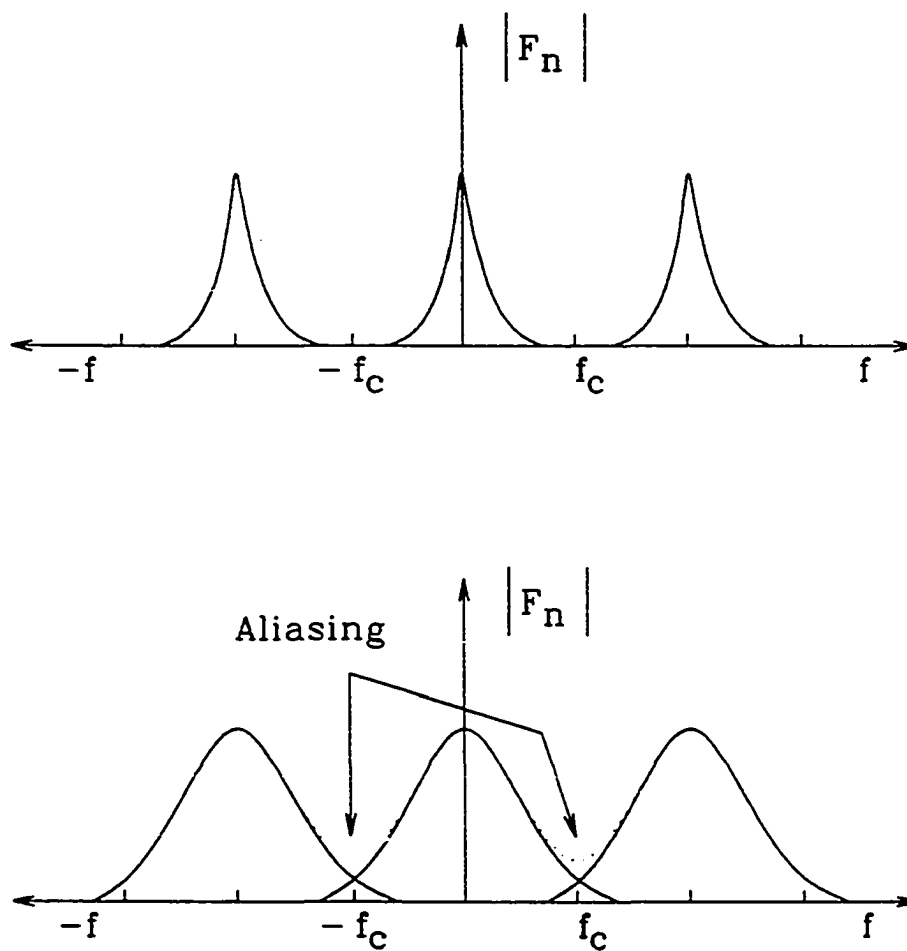


Figure 18. The top figure shows a correctly sampled signal, while the bottom figure shows the aliasing effects of under sampling the signal.

represents an under sampled signal. Notice how the spectrums overlap and "inflate" spectral components through aliasing, introducing an error in the spectral representation.

An easy method of detecting, if enough sampling points have been used, is as follows. After generating a time domain signal, fast Fourier transform the signal to the frequency domain and plot the magnitude of the spectrum. If the spectrum plot decays to zero before the ends of the plot limits, then the selected sample rate is safe to use (note that if the plot appears as a virtual delta function, the number of samples can probably be reduced, speeding execution time). If however, the spectrum is non-zero at the Nyquist frequency, then the number of sample points must be increased.

## CHAPTER 9

## EXPERIMENTAL MEASUREMENT AND SIMULATION COMPARISON

This chapter compares the simulated results with the experimental measurements of a microstrip system. The microstrip structure was built by Advanced Packaging Systems and measurements performed by Cascade Microtech. The modeling of the microstrip was conducted in two phases, RLC parameter extraction (quasi-TEM, dispersive model) and simulation. The frequency dependent resistive and inductive parameters were extracted using the software tool UA3DL2.0, while the non-frequency dependent capacitance was calculated with the tool UAMOM. The simulation was based on techniques discussed in the preceding chapters. An additional structure was simulated by IBM on their transmission line simulator, ASTAP, to obtain time domain transient analysis comparisons. Good agreement was achieved.

## 9.1 Experimental S-parameter Measurements

Experimental S-parameter data was obtained using the thin film High Frequency Test Pattern HFTP-02 fabricated by Advanced Packaging Systems, HDI division of San Jose, CA. Figure 19 shows the configuration of the two test patterns utilized. The structure is composed of five 1.5 inch microstrip segments connected end to end, so that if straightened, would be 7.5 inches long. The aluminum microstrip, embedded in a polyimide with a

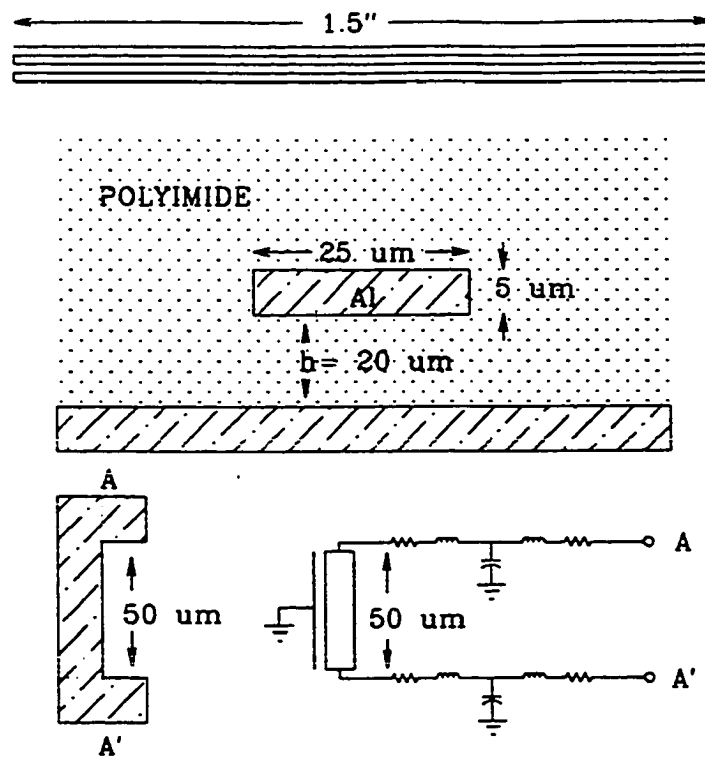


Figure 19. Thin film multilayer high frequency test structure.

relative dielectric constant of 3.4, has the dimensions of width = 25  $\mu\text{m}$ , thickness = 5  $\mu\text{m}$ , height (from ground plane) = 10 and 20  $\mu\text{m}$  and line pitch of 75  $\mu\text{m}$ . The peripheral 16 mil square contact pads are connected through 35  $\mu\text{m}$  diameter vias to the microstrip and are designed for use with the Cascade Microtech Hybrid Probe Station (Cascade Microtech, Inc., Beaverton, OR). The entire structure is mounted on a ceramic substrate.

The measurements were conducted at Cascade Microtech. The measurement station utilizes a Hewlett-Packard HP-8510 network analyzer in conjunction with the Cascade Microtech Hybrid Probe Station. Sampled data is transferred to a Macintosh Plus microcomputer via an IEEE 488 bus for processing. S-parameter measurements were conducted from 100 Hz to 10 GHz. The resulting S11 and S12 measurements are shown in Figures 20 and 21 for a height of 10 and 20  $\mu\text{m}$  respectively.

## 9.2 Simulation

The modeling of the microstrip was conducted in two phases, RLC parameter extraction followed by S-parameter analysis utilizing the extracted parameters for the overall system response. The frequency dependent resistive and inductive parameters were extracted using the software tool UA3DL2.0<sup>21</sup>, while the non-frequency dependent capacitance was calculated with the tool UAMOM<sup>28</sup>. The system response was then simulated with the S-parameter program SPTLA (see chapter 8).

The microstrip was broken up into three components: a 1.5" coupled

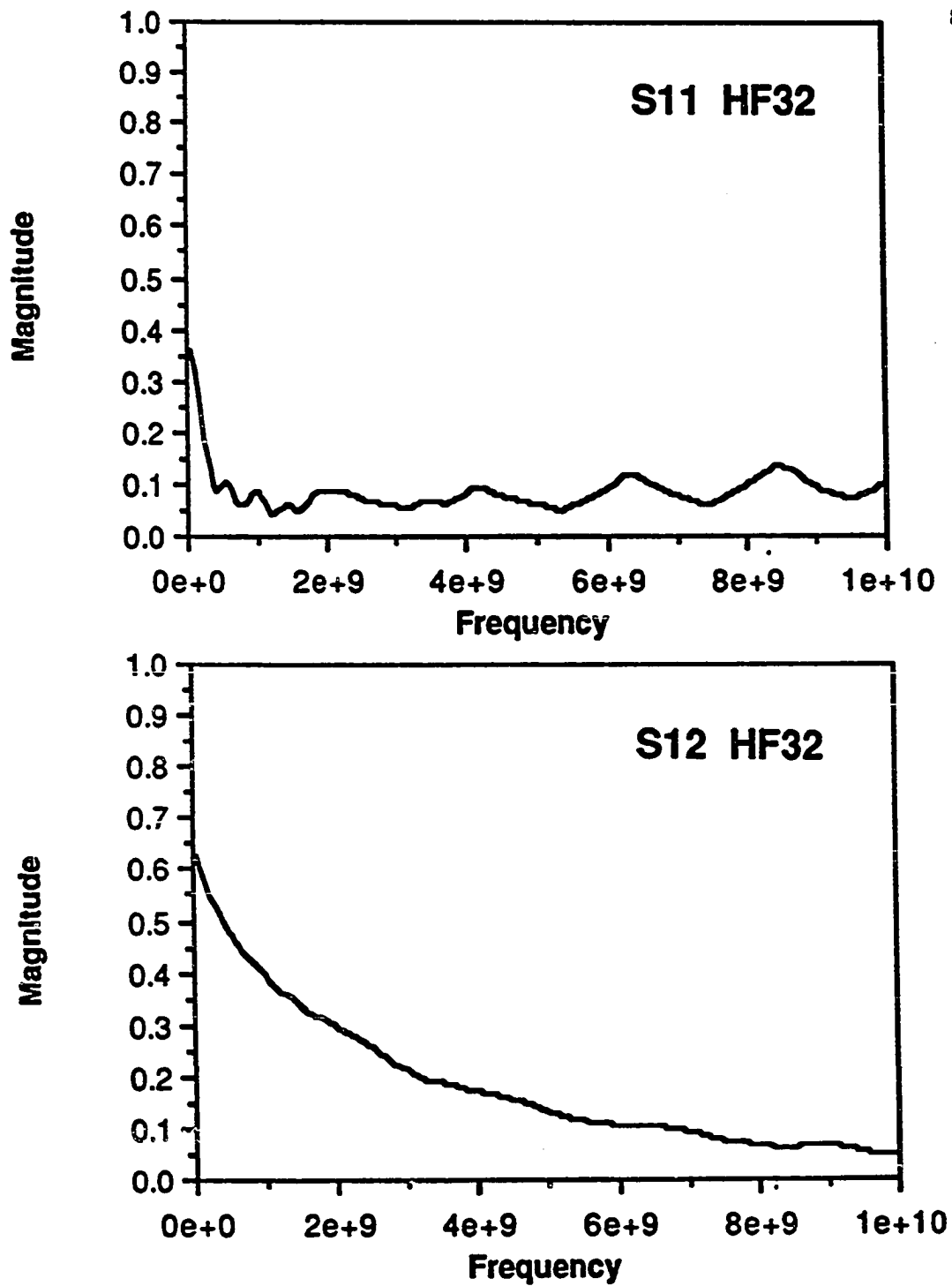


Figure 20. S11, S12 S-parameter measurement,  $h=10 \mu\text{m}$ .

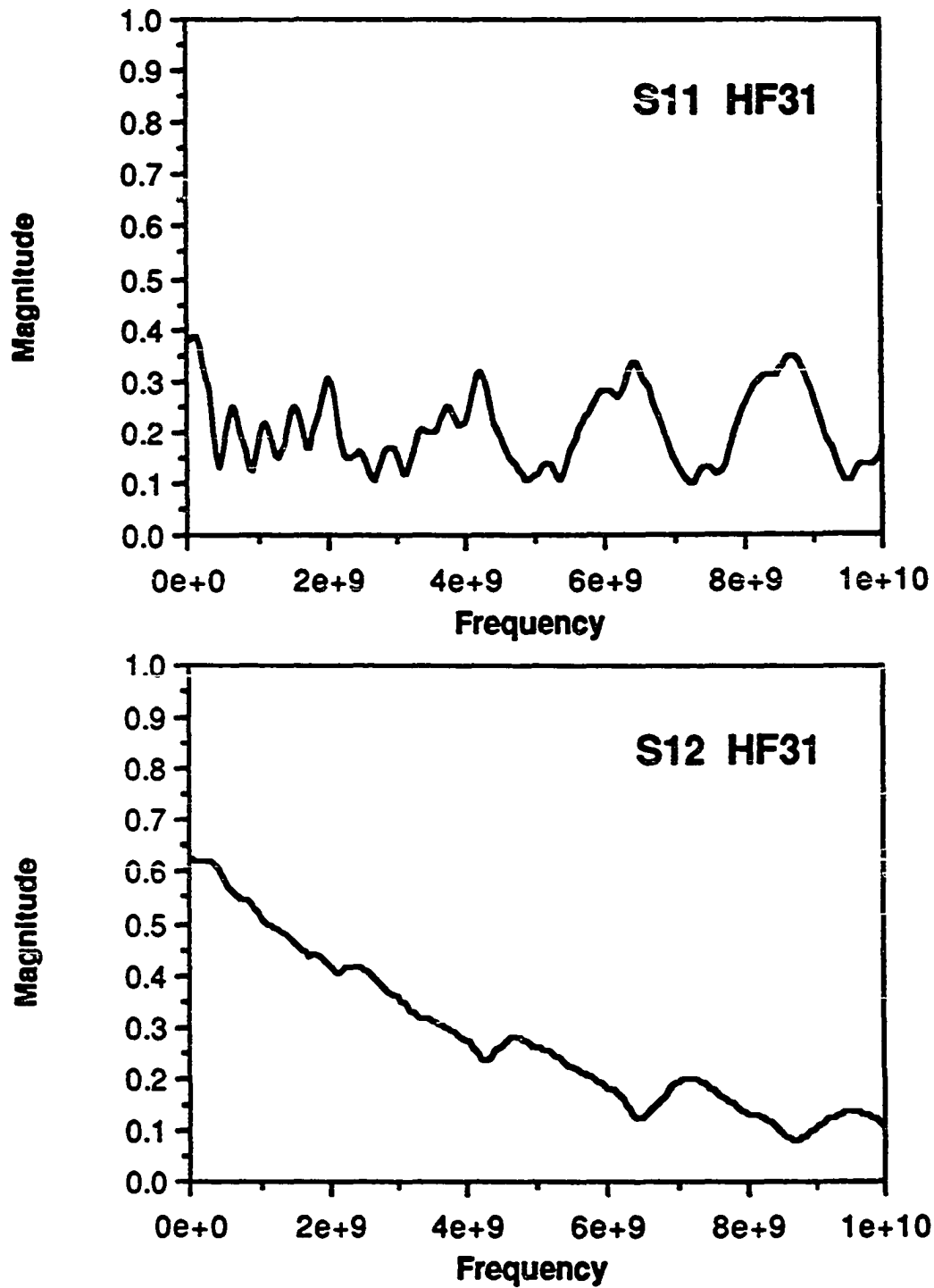


Figure 21. S11, S12 S-parameter measurement,  $h=20 \mu\text{m}$ .

five line system, the 90° bend and the 50  $\mu\text{m}$  transmission line joining the two bends creating the overall 180° bend.

The resulting frequency dependent coupled line RLC matrices are:

$h=10 \mu\text{m}$ :

$$\begin{bmatrix} R(\omega) & 0 & 0 & 0 & 0 \\ 0 & R(\omega) & 0 & 0 & 0 \\ 0 & 0 & R(\omega) & 0 & 0 \\ 0 & 0 & 0 & R(\omega) & 0 \\ 0 & 0 & 0 & 0 & R(\omega) \end{bmatrix} \quad \Omega/\text{m}$$

$$\begin{bmatrix} L(\omega) & 11 & 2.8 & 1.3 & 0.7 \\ 11 & L(\omega) & 11 & 2.8 & 1.3 \\ 2.8 & 11 & L(\omega) & 11 & 2.8 \\ 1.3 & 2.8 & 11 & L(\omega) & 11 \\ 0.7 & 1.3 & 2.8 & 11 & L(\omega) \end{bmatrix} \quad \text{nH/m}$$

$$\begin{bmatrix} 154 & -6.22 & -0.54 & -0.22 & -0.15 \\ -6.22 & 153 & -5.86 & -0.48 & -0.22 \\ -0.54 & -5.86 & 158 & -5.86 & -0.54 \\ -0.22 & -0.48 & -5.86 & 153 & -6.22 \\ -0.15 & -0.22 & -0.54 & -6.22 & 154 \end{bmatrix} \quad \text{pF/m}$$

where:

$$R(\omega) = 228.8848 + 1.078846 \cdot 10^{-8} \omega - 4.8255311 \cdot 10^{-20} \omega^2 \\ + 3.979675 \times 10^{-32} \omega^3 \quad \Omega/\text{m}$$

$$L(\omega) = 2.84178 \cdot 10^{-7} - 1.377801 \cdot 10^{-19} \omega + 1.5230336 \cdot 10^{-29} \omega^2 \\ - 1.464733 \cdot 10^{-42} \omega^3 \quad \text{H/m}$$

$h = 20 \mu\text{m}$ :

$$\begin{bmatrix} R(\omega) & 0 & 0 & 0 & 0 \\ 0 & R(\omega) & 0 & 0 & 0 \\ 0 & 0 & R(\omega) & 0 & 0 \\ 0 & 0 & 0 & R(\omega) & 0 \\ 0 & 0 & 0 & 0 & R(\omega) \end{bmatrix} \quad \Omega/\text{m}$$

$$\begin{bmatrix} L(\omega) & 32 & 8.8 & 4 & 2.3 \\ 32 & L(\omega) & 32 & 8.8 & 4 \\ 8.8 & 32 & L(\omega) & 32 & 8.8 \\ 4 & 8.8 & 32 & L(\omega) & 32 \\ 2.3 & 4 & 8.8 & 32 & L(\omega) \end{bmatrix} \quad \text{nH/m}$$

$$\begin{bmatrix}
 98.8 & -7.46 & -0.6 & -0.27 & -0.2 \\
 -7.46 & 97.0 & -7.6 & -0.51 & -0.27 \\
 -0.6 & -7.6 & 109.1 & -7.6 & -0.6 \\
 -0.27 & -0.51 & -7.6 & 97.0 & -7.46 \\
 -0.2 & -0.27 & -0.6 & -7.46 & 98.8
 \end{bmatrix} \text{ pF/m}$$

where:

$$\begin{aligned}
 R(\omega) = & 234.9468 + 1.034233 \cdot 10^{-8} \omega - 5.0180559 \cdot 10^{-20} \omega^2 \\
 & + 4.227842 \times 10^{-32} \omega^3 \quad \Omega/\text{m}
 \end{aligned}$$

$$\begin{aligned}
 L(\omega) = & 3.86591 \cdot 10^{-7} - 9.773531 \cdot 10^{-19} \omega + 1.0132992 \cdot 10^{-29} \omega^2 \\
 & - 9.683504 \cdot 10^{-42} \omega^3 \quad \text{H/m}
 \end{aligned}$$

are third order power series expansions in  $\omega$  to incorporate the frequency dependent effects which, for this particular system, are significant only in the diagonal elements.

The 180° bend is composed of two 90° bends and a 50  $\mu\text{m}$  transmission line segment. The 90° bends are treated as discontinuities and modeled as frequency dependent T-network (see Chapter 7), while the 50  $\mu\text{m}$  line segment is assumed decoupled and modeled as a single transmission line.

The line segment parameters are

h=10  $\mu\text{m}$ :

$$R(\omega) = 231.612277 + 1.032463 \cdot 10^{-8} \omega - 4.146360 \cdot 10^{-20} \omega^2 \\ + 3.3109541 \cdot 10^{-32} \omega^3 \quad \Omega/\text{m}$$

$$L(\omega) = 2.786642 \cdot 10^{-7} - 1.012947 \cdot 10^{-18} \omega + 1.0310565 \cdot 10^{-29} \omega^2 \\ - 9.831333 \cdot 10^{-42} \omega^3 \quad \text{H/m}$$

$$C = 1.54626 \cdot 10^{-10} \quad \text{F/m}$$

h=20  $\mu\text{m}$ :

$$R(\omega) = 234.759128 + 0.897775 \cdot 10^{-8} \omega - 2.524983 \cdot 10^{-20} \omega^2 \\ + 1.7359010 \cdot 10^{-32} \omega^3 \quad \Omega/\text{m}$$

$$L(\omega) = 3.867432 \cdot 10^{-7} - 0.904653 \cdot 10^{-18} \omega + 0.88360016 \cdot 10^{-29} \omega^2 \\ - 8.388783 \cdot 10^{-42} \omega^3 \quad \text{H/m}$$

$$C = 0.98379 \cdot 10^{-10}, \quad \text{F/m}$$

while the 90° bend discontinuity RLC parameters, which were fit to first order in  $\omega$ , are

h=10  $\mu\text{m}$ :

$$R(\omega) = 1.44608 \cdot 10^{-3} + 4.857766 \cdot 10^{-13} \omega \quad \Omega$$

$$L(\omega) = 1.401868 \cdot 10^{-12} + 1.41429 \cdot 10^{-22} \omega \quad \text{H}$$

$$C = 2.714 \cdot 10^{-15} \quad \text{F}$$

h=20  $\mu\text{m}$ :

$$R(\omega) = 1.62020 \cdot 10^{-3} + 1.380604 \cdot 10^{-12} \omega \quad \Omega$$

$$L(\omega) = 1.475590 \cdot 10^{-12} + 5.73426 \cdot 10^{-22} \omega \quad \text{H}$$

$$C = 1.665 \cdot 10^{-15} \quad \text{F}$$

It should be noted that the above power series expansions are valid only over the range of zero to 15 GHz.

The coupled line system was then simulated on SPTLA. The simulated S11, S12 for h=10 and 20  $\mu\text{m}$ , denormalized to 80  $\Omega$ , are shown in Figures 22-23 and agree well with the measured data. While the simulation was successfully carried out to 10 GHz for this case, in general the validity of simulations beyond 2 to 3 GHz must be questioned. Note that the reason such high frequency components are required for a time domain simulation

is due to the Fourier techniques used. For an  $N$  point FFT, the highest frequency component required is  $N/2$  times the period (see Chapter 8 on Fourier aliasing). The simulation used in this example has  $N=256$ , hence, for a 10 GHz maximum, the period (or clock rate) is 78.125 MHz. However, for the typical clocked signals used in VLSI systems, only the first 4 to 5 frequency components of the transformed pulse contain significant power (see Chapter 6). Hence, for this example, only the 1<sup>st</sup> GHz of S11 and S12 need be accurate.

An example of a time domain response of the microstrip of Figure 18 (utilizing the S-parameters of Figures 4 and 5) is shown in Figure 24. The Figure shows the input (periodic) pulse and the propagating pulse at each bend for 50  $\Omega$  source and load terminations. Note the signal attenuation attributed to line losses.

Due to the unavailability of measured time domain data of coupled transmission lines, comparisons were made with IBM's ASTAP time domain transmission line simulator. Figure 25 provides a schematic of the network. There are two 3-line lossless coupled transmission lines that are each one inch in length with L and C matrices

$$\begin{bmatrix} 0.667 & -0.163 & -0.015 \\ -0.163 & 0.722 & -0.163 \\ -0.015 & -0.163 & 0.667 \end{bmatrix} \text{ pF/cm}$$

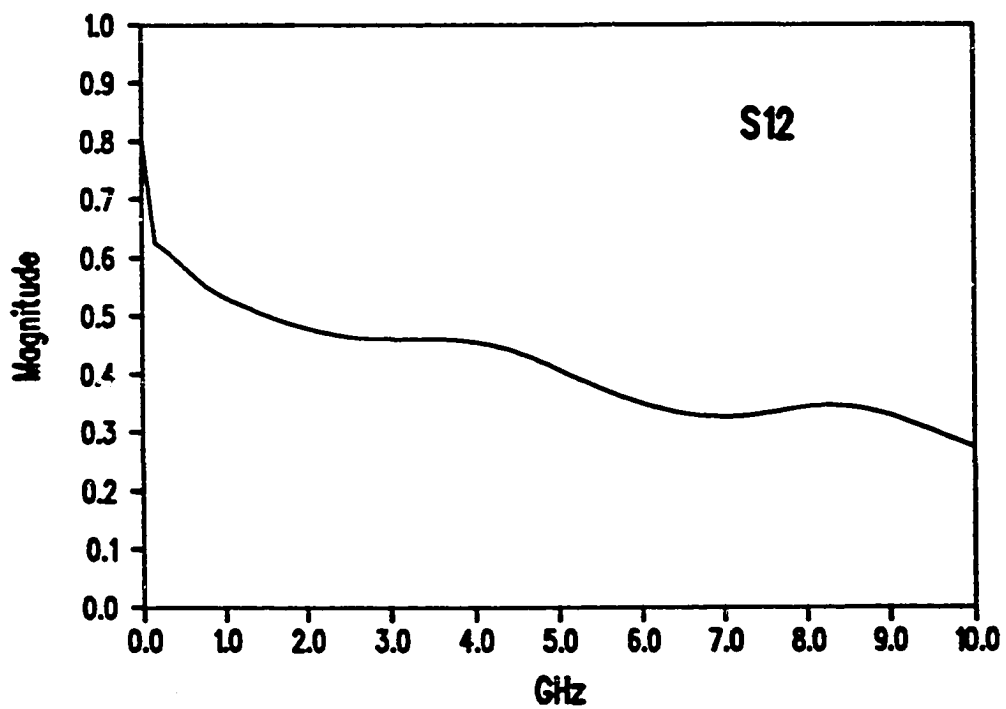
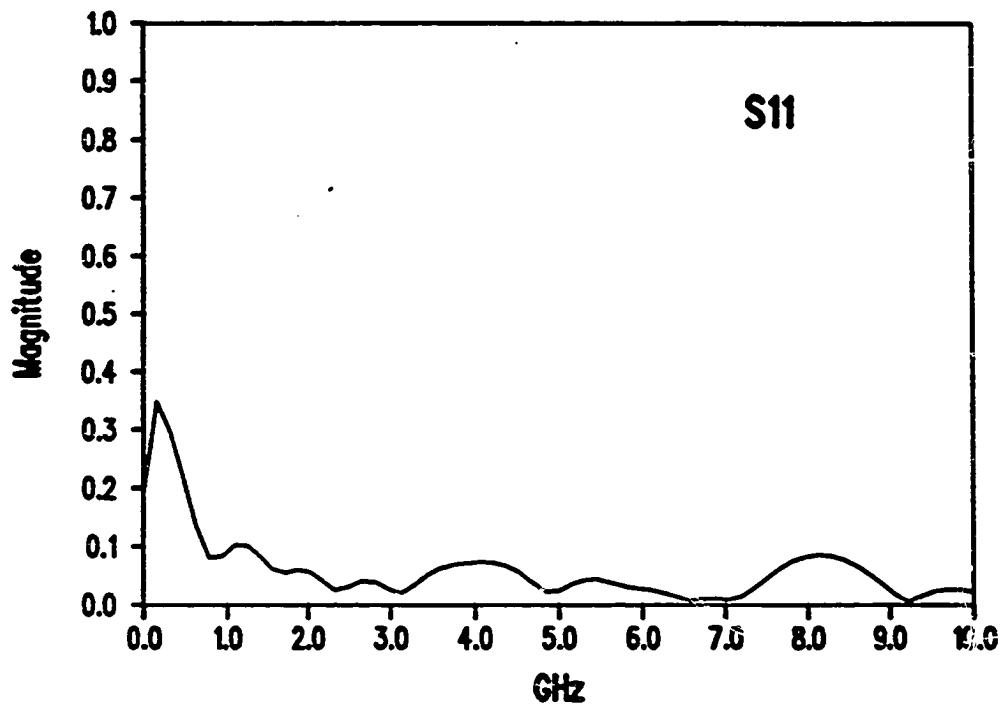


Figure 22. S11, S12 S-parameter simulation,  $h=10 \mu\text{m}$ .

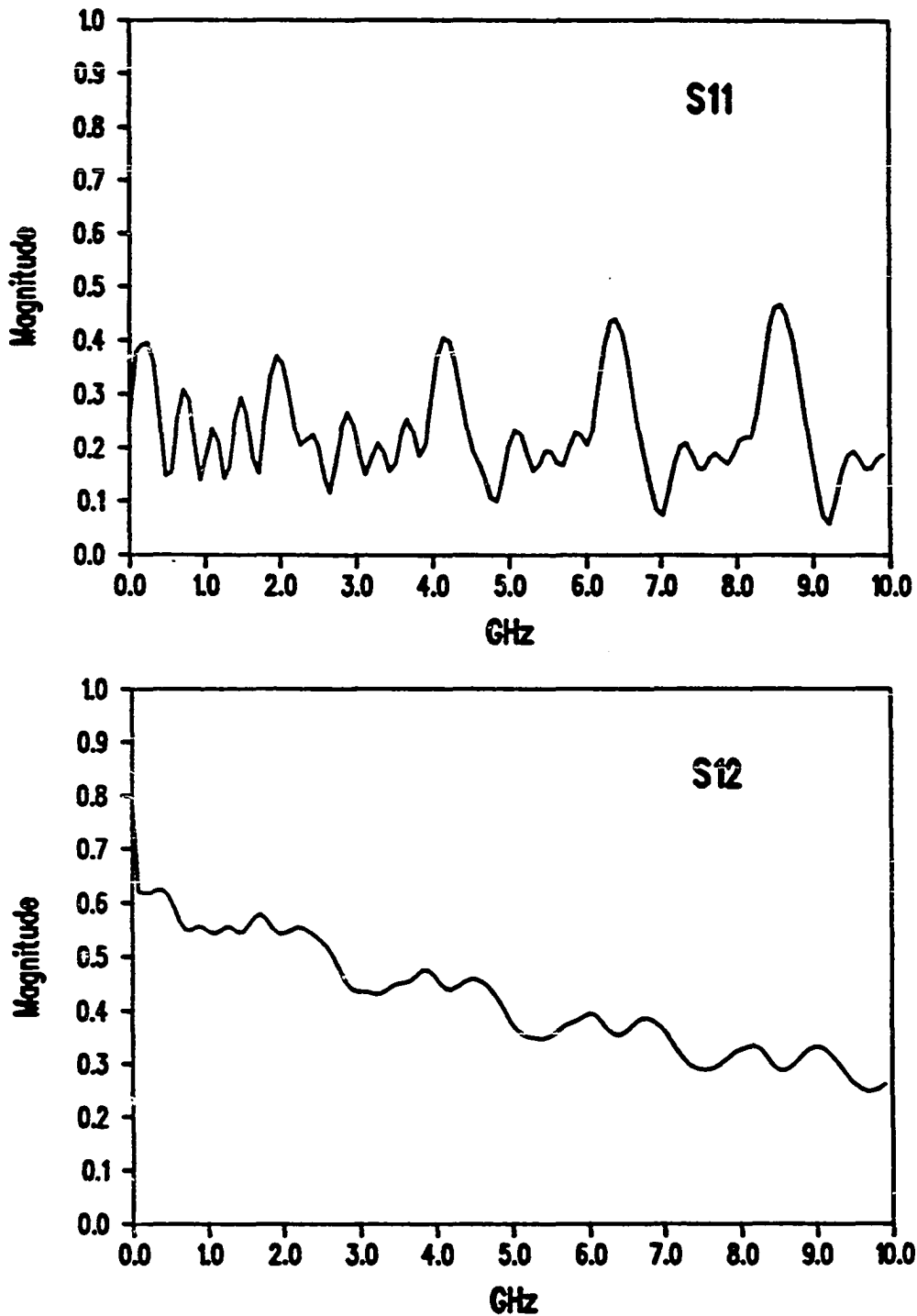


Figure 23. S11, S12 S-parameter simulation,  $h=20 \mu\text{m}$ .

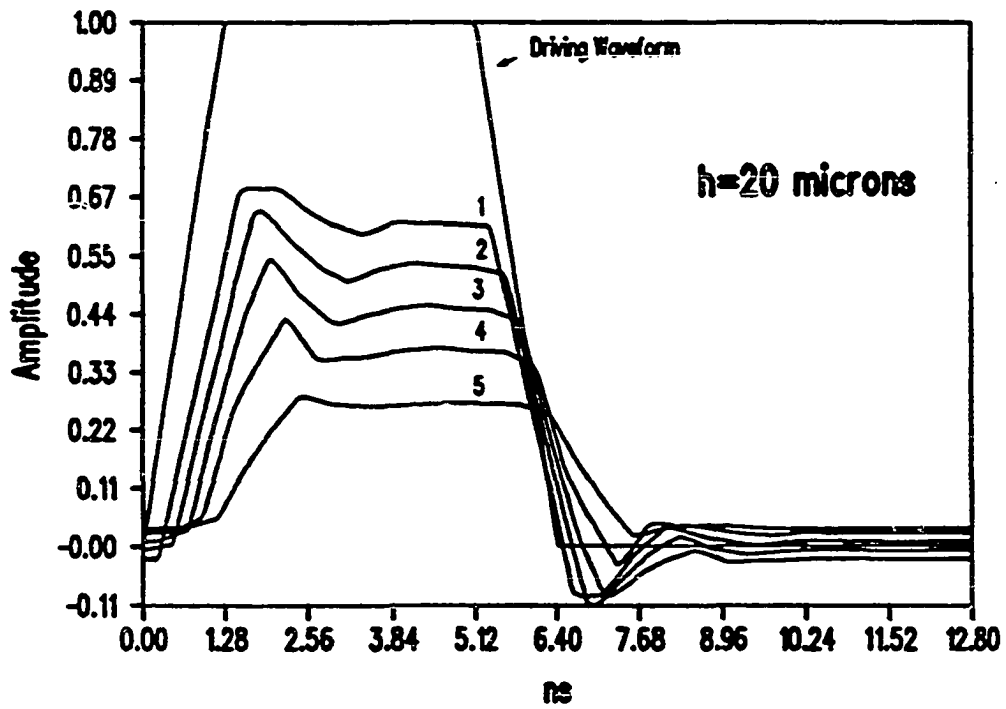
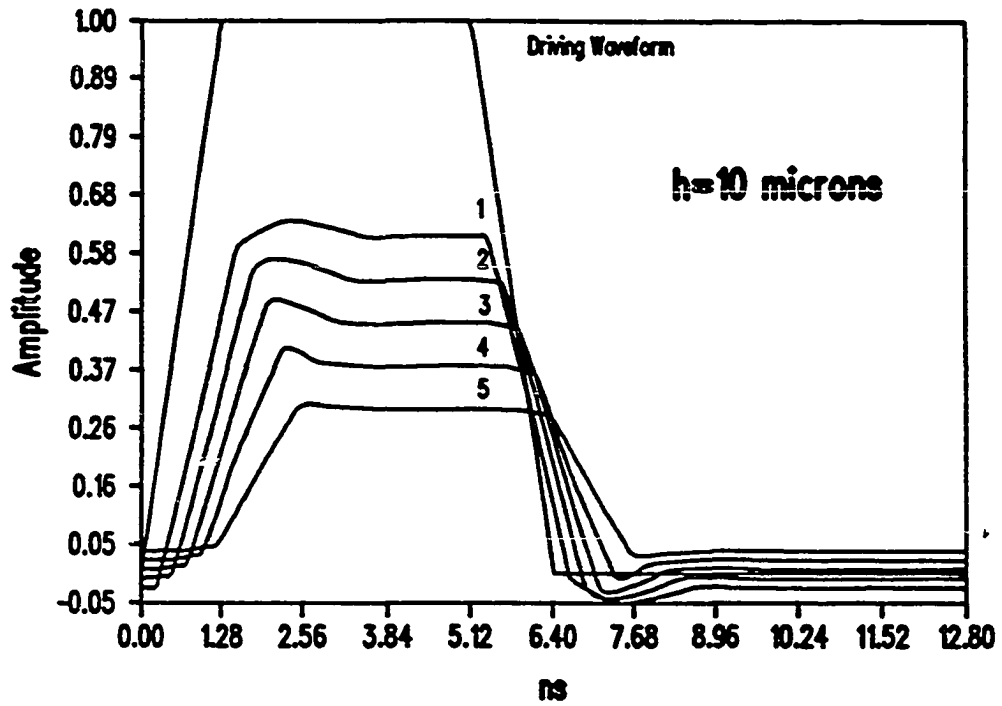


Figure 24. Time domain propagation of pulse for  $50 \Omega$  terminations.

$$\begin{bmatrix} 5.033 & 1.734 & 0.818 \\ 1.734 & 4.972 & 1.734 \\ 0.818 & 1.734 & 5.033 \end{bmatrix} \text{ nH/cm}$$

The center line is active and the two outer lines represent a shield line and a coupled load line. The active line is driven by a clocked source at a frequency of 100 MHz with a rise time of 0.1 ns. The resulting SPTLA simulation along with the ASTAP simulation is shown in Figure 26. It should be noted that ASTAP is a time domain transient analysis program and Figure 26 shows the simulation results of a sequence of ten pulse cycles.

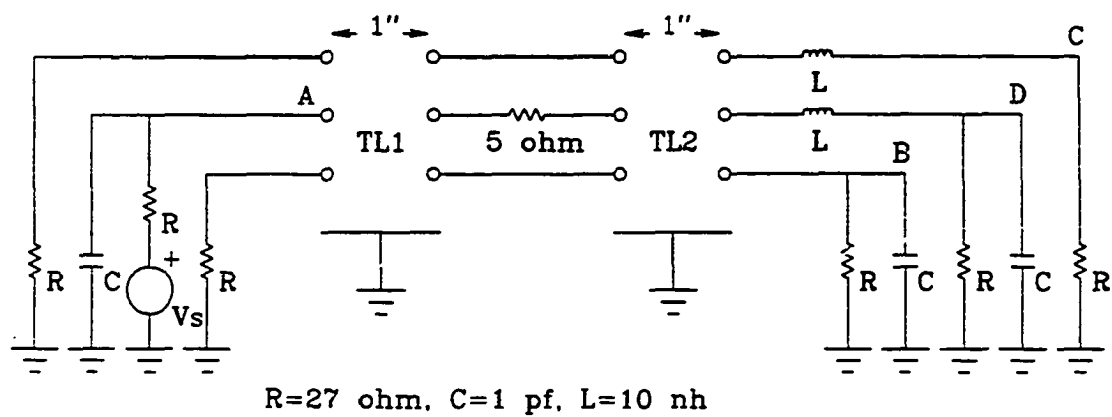
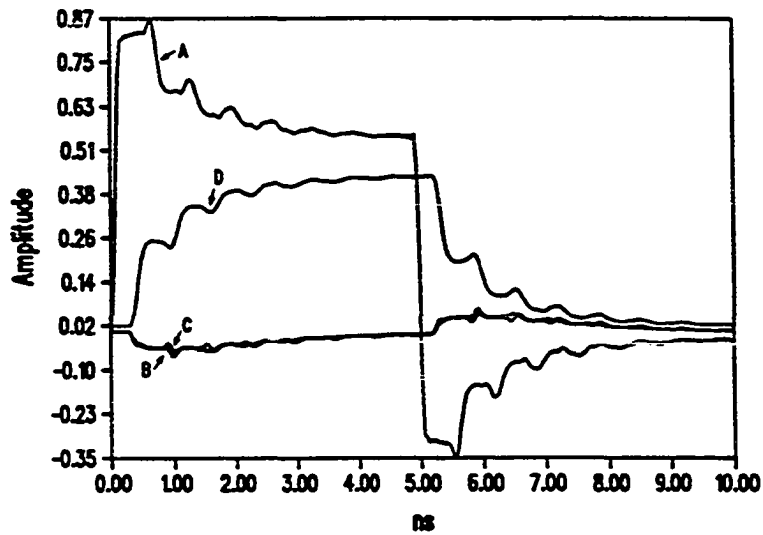


Figure 25. Network schematic of time domain simulation.



IBM

RCAID W08752 APR 18 1989 12:43:21  
 100 MHz Clock, .1 ns Rise Time  
 Figure 10-a

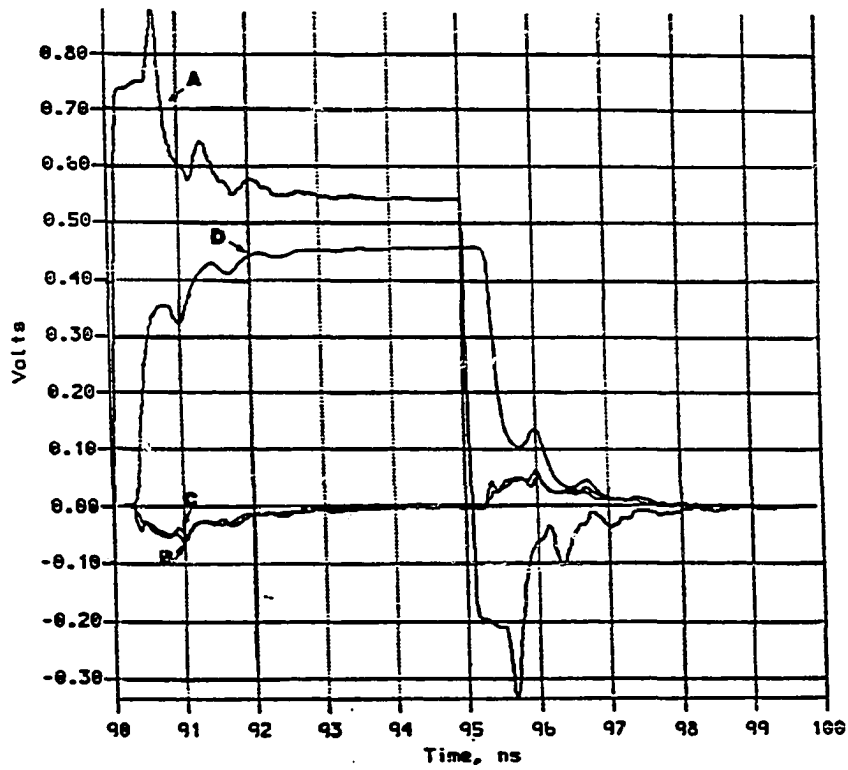


Figure 26. Network response for 100 MHz clock with 0.1 ns rise time.

**CHAPTER 10****CONCLUSION**

The implementation of S-parameter techniques for the analysis of high speed integrated circuit and packaging interconnects has been investigated. An algorithm has been developed that allows for the inclusion of frequency dependent parameters, analysis of periodic waveform response and the incorporation of measured or externally calculated S-parameter data into an analysis. Verification of the algorithm has been shown through comparisons with experimentally obtained data and another transmission line analysis program. An algorithm to incorporate non-linear terminations has been developed.

This dissertation primarily establishes S-parameter techniques as a viable tool for the computer aided analysis and design of high speed integrated circuits and packaging interconnects. The next phase of research should investigate and develop the potential applications that are unique to S-parameter techniques. Future research should include incorporation of non-TEM structures, large system decomposition and lossy line engineering. Appendix A describes the latter two of these S-parameter applications.

**APPENDIX A: S-PARAMETER APPLICATIONS**

This appendix briefly describes two potential S-parameter applications: lossy line engineering and large system decomposition.

The simple transmission line system shown in Figure 27 can be used to illustrate the potential uses of deliberately introduced line losses. The transmission line parameters are those of the decoupled frequency dependent line ( $h=20\ \mu\text{m}$ ) discussed above. The lines are 10 cm long and are terminated in 1 pf and 5 pf capacitors for the upper and lower branch respectively and are driven by a matched source. Figures 28 and 29 show the response of the frequency dependent lossy and lossless system across the 1 pf capacitor (node A). Both Figures 28 and 29 show the response of a system driven by a clock with 1 ns rise and fall times and a 1 volt amplitude. However, the clock rate for Figure 28 is 100 MHz while that of Figure 29 is 10 MHz. Note the great difference in response between the lossless and lossy system. While the lossy system tracks the 1 ns rising and falling edges of both clock frequencies reasonably well, the response of the lossless system is severely degraded. This would suggest that systems with relatively large discontinuities or termination mismatches like those found in high speed CMOS and III-V compound circuits (which have capacitive inputs) could benefit from losses through damping. Careful line loss engineering may be used to enhance system performance.

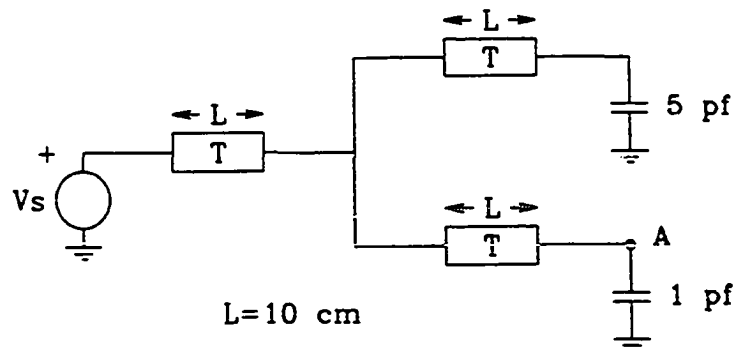


Figure 27. Transmission line system used to illustrate effects of line losses.

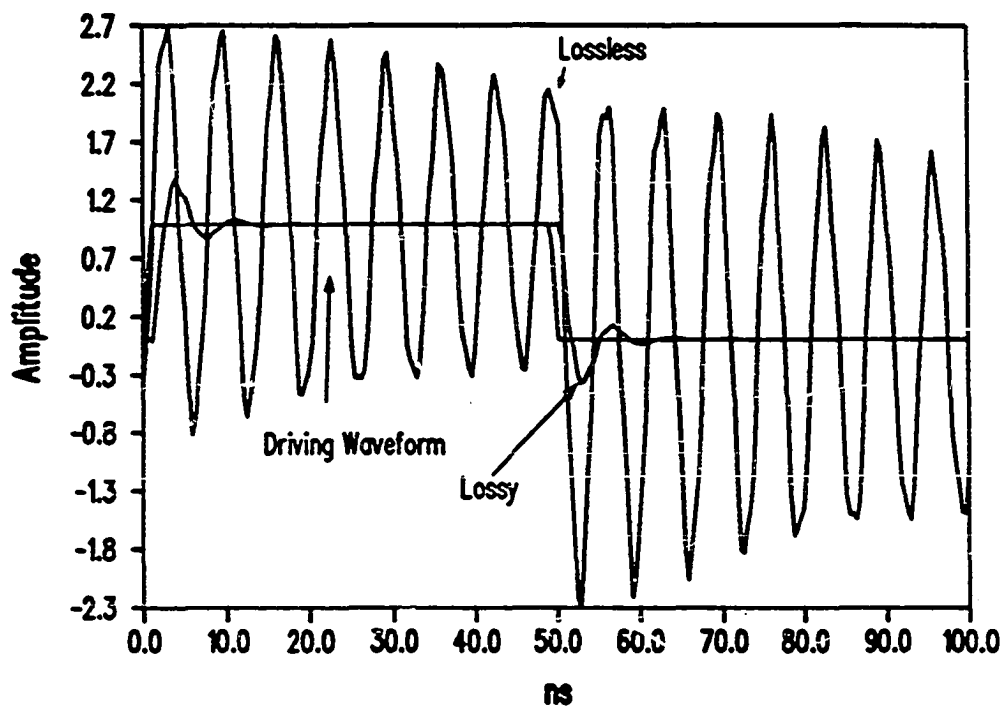


Figure 28. 10 MHz pulse train far end response (node A).

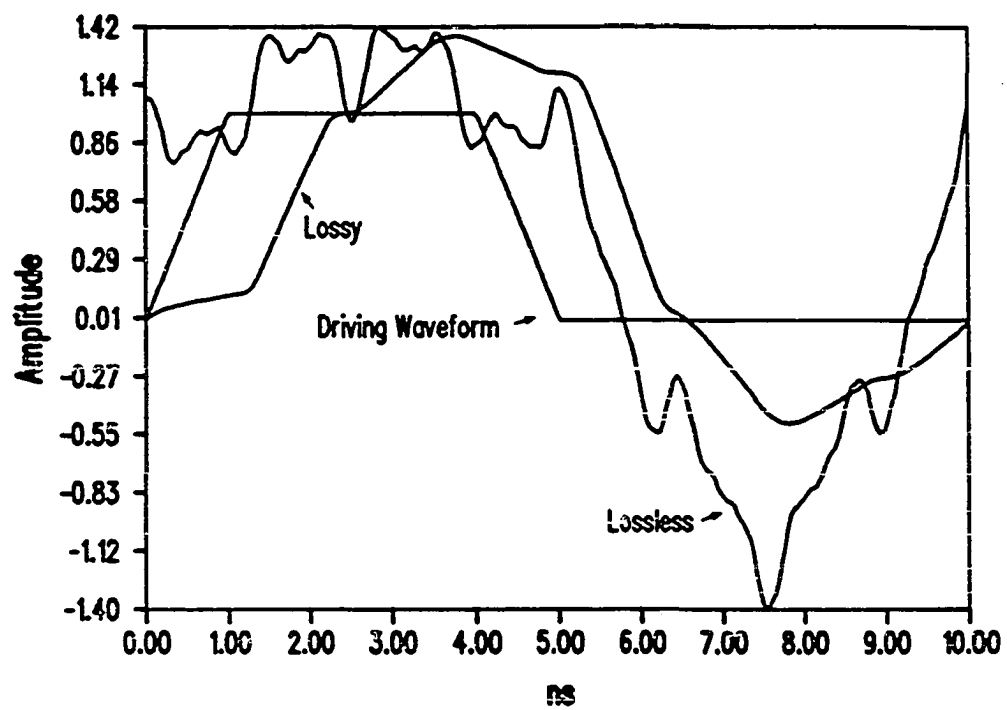


Figure 29. 100 MHz pulse train far end response (node A).

Network S-parameter analysis allows a system to be decomposed and analyzed as subsystems and later reconstituted with the much smaller subsystem network. Such a technique would allow very large systems to be rapidly evaluated on common computers and minimizes the problems associated with inverting very large matrices. In addition, many large interconnect systems are composed of redundant geometries. S-parameters for redundant elements such as bends, vias and coupled line segments need only be evaluated once and stored as a macro to be called when needed. An example of system decomposition was illustrated by the microstrip analysis given in chapter 9. The 22 port microstrip bend circuit, shown in Figure 30, is replaced by its equivalent two port macro. The macro is then inserted into the coupled five conductor microstrip for the overall circuit response as shown in Figure 31. Note that by using the macro, the simulation requirements are reduced from 95 ports to 23 ports.

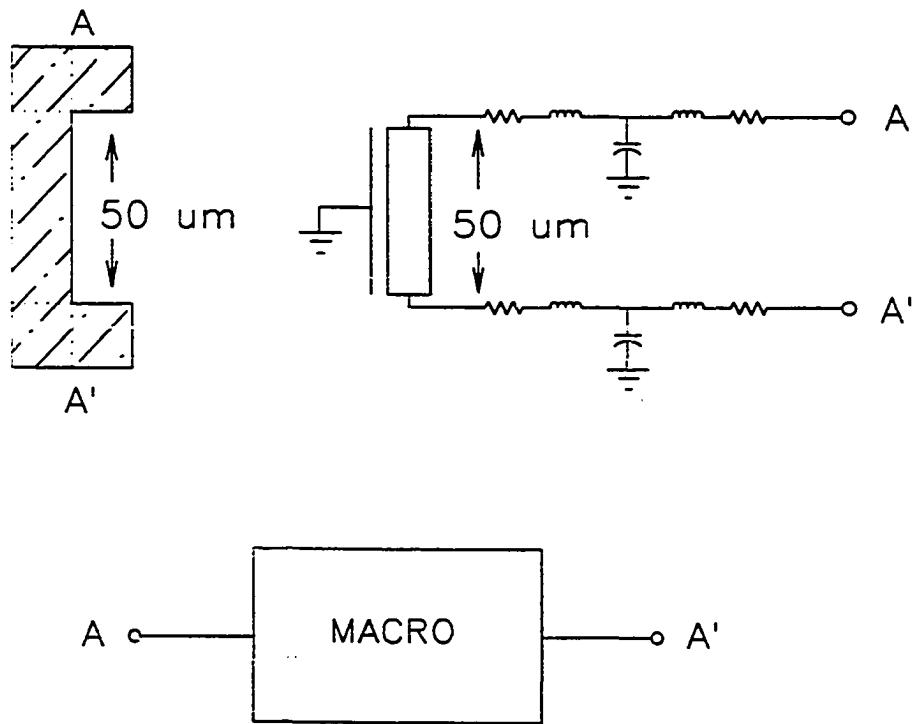


Figure 30. The equivalent two port macro for a microstrip bend.

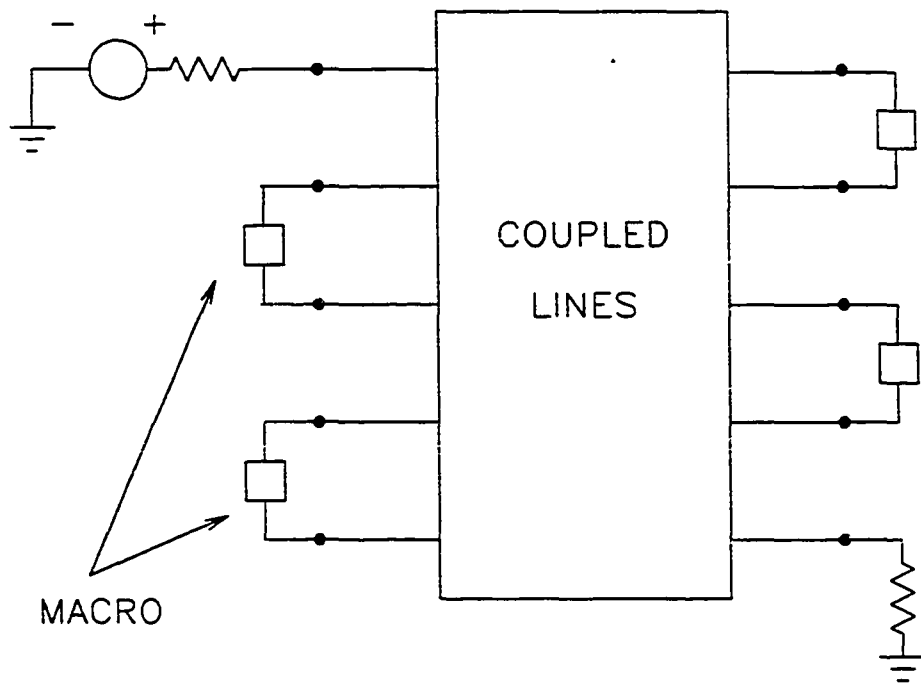


Figure 31. Coupled five conductor microstrip simulation with using macros.

## REFERENCES

1. K. C. Gupta, R. Garg, I. J. Bahl, "Microstrip Lines and Slotlines", Artech, 1979, pp. 4-7.
2. P. A. Rizzi, "Microwave Engineering", EnglewoodCliffs, N. J., 1938, pp. 541-548.
3. K. C. Gupta, R. Garg, R. Chadha, "Computer-Aided Design of Microwave Circuits", Artech, 1981, pp. 338-347.
4. R. W. Newcomb, "Linear Multiport Synthesis", McGraw-Hill, 1966, pp. 64-78.
5. V. A. Monaco and P. Tiberio, "Computer-Aided Analysis of Microwave Circuits", IEEE Trans. Microwave Theory and Techniques, MTT-22, March 1974, pp. 249-263.
6. R. W. Newcomb, "Linear Multiport Synthesis", McGraw-Hill, 1966, pp. 46-57.
7. K. C. Gupta, R. Garg, R. Chadha, "Computer-Aided Design of Microwave Circuits", Artech, 1981, pp. 30-42.
8. K. C. Gupta, R. Garg, R. Chadha, "Computer-Aided Design of Microwave Circuits", Artech, 1981, pp.40-43.
9. A. R. Djordjevic and T. K. Sarkar, "Analysis of Time Response of Lossy Multiconductor Transmission Line Networks", IEEE Trans. Microwave Theory and Techniques, MTT-35, Oct. 1987, pp. 898-908.
10. H. Amemiya, "Multiple Parallel Transmission Lines", RCA REVIEW, June 1967. pp.241-277.
11. J. D. Jackson, "Classical Electrodynamics", John Wiley & Sons, 1975, 2<sup>nd</sup> edition, pp. 369-375.
12. L. Carin, K. J. Webb, "Characteristic Impedance of Multilevel, Multiconductor Hybrid Mode Microstrip", IEEE Trans. Magnetics, 25, July 1989, pp. 2947-2949.
13. R.W. Newcomb, "Linear Multiport Synthesis", McGraw-Hill, 1966, pp. 73-76.

14. A. R. Djordjevic, T. K. Sarakar and R. F. Harrington, "Analysis of Lossy Transmission Lines with Arbitrary Nonlinear Terminal Networks", IEEE Trans. Microwave Theory and Techniques, MTT-34, June 1986, pp. 660-666.
15. K. C. Gupta, R. Garg, I. J. Bahl, "Microstrip Lines and Slotlines", Artech, 1979, chpt. 2.
16. F. B. Hildebrand, "Advanced Calculus for Applications", 2<sup>nd</sup> ed., Prentice-Hall, 1976, pp. 219-223.
17. F. G. Stremmer, "Introduction to Communication Systems", 2<sup>nd</sup> ed., Addison-Wesley Publishing Company, 1982, pp. 99-101.
18. F. B. Hildebrand, "Advanced Calculus for Applications", 2<sup>nd</sup> ed., Prentice-Hall, 1976, pg. 256.
19. F. G. Stremmer, "Introduction to Communication Systems", 2<sup>nd</sup> ed., Addison-Wesley Publishing Company, 1982, pp. 17-23.
20. J. D. Jackson, "Classical Electrodynamics", John Wiley & Sons, 1975, 2<sup>nd</sup> edition, pp. 236-244.
21. A. C. Cangellaris, J. L. Prince, L. Vakanas, "Frequency-Dependent Inductance and Resistance Calculation for Three-Dimensional Structures in High-Speed Interconnect Systems", Proc. of the 1989 39<sup>th</sup> IEEE Electronics Components Conference, pp. 398-403, May 1989.
22. M. R. Scheinfein, J. L. Prince, "Electrical Performance of Integrated Circuit Packages: Three Dimensional Structures", Proc. of the 1987 37<sup>th</sup> IEEE Electronics Components Conference, pp. 377-383, May 1987.
23. K. C. Gupta, R. Garg, R. Chadha, "Computer-Aided Design of Microwave Circuits", Artech, 1981, pp. 39-42.
24. K. C. Gupta, R. Garg, P. Chadha, "Computer-Aided Design of Microwave Circuits", Artech, 1981, pp. 179-199.
25. W. H. Press, B. P. Flannery, S. A. Teukolsky, W. T. Vetterling, "Numerical Recipes", Cambridge University Press, 1986, pp.31-39.
26. Applied Mathematics Division, Argonne National Laboratory.
27. A. V. Oppenheim, R. W. Schaffer, "Digital Signal Processing", Prentice-Hall, 1975, 6-30.

28. M. R. Scheinfein, J. C. Liao, O. A. Palusinski and J. L. Prince, "Electrical Performance of High Speed Interconnect Systems", IEEE Trans. Components, Hybrids and Manufacturing Technology CHMT-10, Sept. 1987, pp. 303-309.